IEEE Access
Multidisciplinary | Rapid Review | Open Access Journal

Received 8 October 2023, accepted 25 October 2023, date of publication 1 November 2023, date of current version 6 November 2023.

Digital Object Identifier 10.1109/ACCESS.2023.3329055

RESEARCH ARTICLE

Adaptive Backstepping Stabilization of Thermoacoustic Instability in a Linearized ODE-PDE Rijke Tube Model

ELHAM AARABI[1], MOHAMMADALI GHADIRI-MODARRES[2], AND MOHSEN MOJIRI[1]
[1]Department of Electrical and Computer Engineering, Isfahan University of Technology (IUT), Isfahan 84156-83111, Iran
[2]Department of Electrical Engineering, Arak University of Technology, Arak, 38181-46763 Iran

Corresponding author: Mohsen Mojiri (mohsen.mojiri@iut.ac.ir)

ABSTRACT This paper proposes an adaptive scheme for the boundary stabilization of thermoacoustic instability in the Rijke tube system using the backstepping method. The mathematical model of the system is characterized by a 2×2 linear hyperbolic partial differential equation (PDE) coupled with a first-order ordinary differential equation (ODE) in a non-strict-feedback form. Recently, a full state feedback controller has been developed to stabilize the system, assuming that the parameters of the model are known. We take into account the most common uncertain parameters which result in the coefficients of the first-order ODE system being unknown parameters. The technique of adaptive identifier is then used along with the normalized gradient algorithm to achieve the parameter update laws. The adaptive control law is obtained by replacing the output of the identifier and estimated parameters in the non-adaptive state feedback control law. The adaptive control law is then manipulated such that it uses a few measurements of the PDE states. According to the stability analysis of the system, the proposed controller guarantees that all closed-loop system states are bounded, while the ODE-PDE system states are convergent to zero. Performance of the proposed scheme is evaluated by the simulation examples.

INDEX TERMS Adaptive stabilization, backstepping method, ODE-PDE system, Rijke tube, thermoacoustic instability.

I. INTRODUCTION

A. MOTIVATION

Thermoacoustic instability phenomenon is a serious challenge affecting the structure of steam and gas turbines, industrial burners, and propulsion systems [1]. This instability arises from the unstable feedback coupling between the heat release rate and acoustic pressure [2]. The Rijke tube is an academic set-up that provides an accessible platform to study the thermoacoustic instability. Fig. 1 illustrates the basic Rijke tube apparatus composed of a vertical open-ended glass tube, with a high length to diameter ratio and a heater coil placed at the lower half of the tube [2]. The coil transfers heat to its adjacent air volume, which then expands and results in acoustic pressure and velocity oscillations [3]. At the heating area, the acoustic pressure perturbs the heat release rate, while the coil feeds energy into the acoustic field, which can lead to their resonant growth. For some critical value of the heat power, the tube will begin to hum loudly, which is the manifestation of instability [2]. A speaker mounted near the bottom of the tube is used as an actuator to suppress the oscillations.

A practical example fitting into the Rijke tube model is the thermoacoustic instability phenomenon happening in the combustion process of the gas turbine engine. As illustrated in Fig. 2, the combustor is an area of the gas turbine where the chemical reaction of fuel and air occurs. The air is supplied by the compressor which increases the air pressure. The combustor adds energy to this pressurized air by spraying fuel and igniting it so that the high-temperature pressurized gas is released. The products of combustion are then converted into work by the turbine. The potential coupling between the

The associate editor coordinating the review of this manuscript and approving it for publication was Zhiguang Feng.

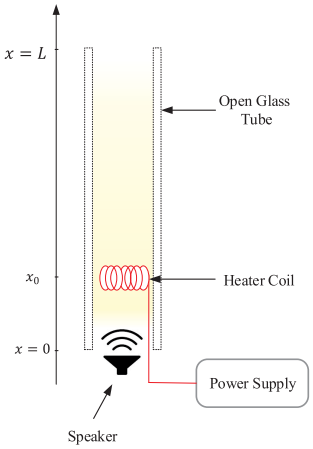

FIGURE 1. Illustration of the main components of the Rijke tube [2].

pressure and heat release rate can generate thermoacoustic instability, which results in large vibrations and damage to the components of the turbine [1]. The feedback control issues appearing in combustion instabilities of gas turbine engine are also present in the Rijke tube experiment [5]. The injection of fuel into the flowing air that causes combustion in the combustor resembles the injection of heat into the air within the Rijke tube. The heat release is dynamically coupled to the acoustic in both systems, which causes thermoacoustic instability.

B. LITERATURE REVIEW

The earliest efforts to stabilize thermoacoustic instability that relies on the finite-dimensional approximation of the system include passive controllers [6], linear quadratic regulator controllers [7], and phase shift controllers [8]. Later, by the continuum backstepping method for the partial differential equations (PDEs), the boundary stabilization of thermoacoustic instability in the Rijke tube modeled by a wave PDE containing a destabilizing term at its uncontrolled boundary has been addressed in [9] and [10]. These studies primarily have assumed that the flame front appears at the boundary. In [11], the Rijke tube with an in-domain heating element is considered, and the boundary feedback control law is designed, which exponentially stabilizes the system. However, the heat release dynamics which models the interaction between the heating element and the surrounding air has been neglected.

Recently, a more realistic model of the Rijke tube system has been taken into account; it considers both the in-domain heating element and the heat release dynamics. The model is described by a 2×2 linear hyperbolic partial differential equation (PDE) coupled with a first-order ordinary differential equation (ODE). The 2×2 PDE acts like a wave equation and represents the dynamics of the acoustic velocity and pressure along the tube, and the ODE models the heat release dynamics. The non-strict-feedback connection between the PDE and ODE, and the Dirac delta distribution applied to model the heat release as a point source term make the design

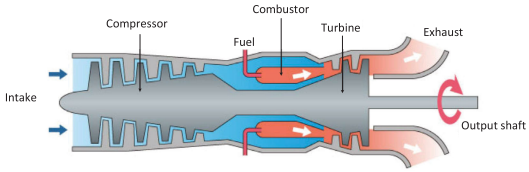

FIGURE 2. Gas-turbine schematic [4].

and analysis more challenging. Assuming the parameters of the model are known, [5] develops a full state feedback boundary controller to stabilize the system by introducing an integral transformation with Volterra and Fredholm terms. However, in practical applications, the mathematical model of the system has uncertain parameters; these include the unknown heat release time constant, the unknown steady-state velocity, and the unknown wire temperature [5]. This motivates us to design an adaptive backstepping controller for the stabilization of the ODE-PDE Rijke tube model.

Adaptive backstepping control of PDEs with uncertain parameters has also been studied in the recent years and several constructive approaches which can be broadly classified as Lyapunov-based design, passivity-based design, and swapping-based design have been developed [12]. For hyperbolic PDEs, adaptive control of a single hyperbolic PDE with a non-local source term has been presented in [13]. The method has been later extended to second-order hyperbolic PDEs [10], 2×2 coupled linear hyperbolic PDEs [14], [15], $n + 1$ coupled linear hyperbolic PDEs [16], and general $n + m$ coupled linear hyperbolic PDEs [17]. Over the last two decades, the backstepping control of ODEs coupled to PDEs with both known and unknown parameters has been extensively investigated in the literature, such as [18], [19], [20], [21], [22], [23], [24], [25], and [26]. Recently, adaptive control of linear 2×2 hyperbolic PDEs coupled with an uncertain ODE has been considered in [27] and [28]. However, in these studies, the ODE-PDE connection is in the strict-feedback form, and the input matrix of the ODE is assumed to be known.

C. CONTRIBUTIONS

This paper focuses on the linearized ODE-PDE model of the Rijke tube system wherein the coefficients of the ODE are unknown. The objective is to design an adaptive control law for the boundary stabilization of the system using the infinite-dimensional backstepping approach. The salient feature of the backstepping method is that it leads to an explicit control law. To design the controller, we do not use the finite-dimensional approximation of the plant by performing spatial discretization. Instead, we develop our adaptive scheme for the nondiscretized plant in the continuum domain, which is more elegant as it is independent of the discretization scheme. Moreover, as mentioned in [12], if one first obtains the spatially discretized version of the plant and then applies finite-dimensional adaptive backstepping methods for ODEs [29], [30], [31], the control gains do not converge upon grid refinement.

There are a number of challenges in the adaptive control of the ODE-PDE Rijke tube model considered in this paper. First, the model has a discontinuity point in the domain that is raised by the Dirac delta distribution. As a consequence, careful attention should be paid when designing the update laws to ensure the boundedness and square integrability of the relevant signals. Second, both the state and input coefficients of the ODE subsystem are unknown and the controller can have access to them through an infinite-dimensional dynamics which has infinite eigenvalues on the imaginary axis [5]. These issues make us follow an identifier-based adaptive control. The proposed adaptive scheme consists of two modules, namely, the adaptive identifier and the controller. The adaptive identifier module has two roles: (i) providing the update laws for the online estimation of the unknown parameters, and (ii) reconstructing the ODE state of the Rijke tube model as the identifier output. The controller module receives the online estimates of the unknown parameters, along with the identifier output, and provides the adaptive control law. This adaptive control law is reformulated, such that it requires a few measurements of the PDE states along the tube.

Another challenging task is to show that the proposed controller-identifier pair guarantees closed-loop stability, which is carried out with a rigorous perspective. Specifically, we propose an infinite-dimensional adaptive backstepping transformation that converts the system along with the control law into a new system called the target system, which is more convenient for stability analysis. The boundedness and regulation of the target system are meticulously laid out with a suitable Lyapunov function. The backstepping transformation is invertible, which enables us to establish the norm equivalence between the target system and the original system. The effects of disturbances, nonlinear heat release dynamics, and actuator dynamics on the performance of the proposed scheme are studied using numerical simulations.
For clarity, the comparisons with the recent results are summarized as follows:

- As compared to the previous results in [32], [33], [34], and [35], which rely on the finite-dimensional approximation of the system, the proposed adaptive scheme takes into account the distributed features of the system. Moreover, using the continuum version of the backstepping method, we meticulously laid out the stability analysis of the complete feedback system consisting of the ODE-PDE Rijke tube model and the proposed infinite-dimensional adaptive control law.
- Different from adaptive control designs [9], [10], this paper focuses on the more realistic model of the Rijke tube system that takes into account the heat release dynamics and both the downstream and upstream parts of the tube. In fact, the plant is extended from an anti-damped wave PDE to the non-strict-feedback connection of a PDE and an ODE, which is more challenging.

TABLE 1. Notation.

Notation	Definition
$\mathbb{R}$	Set of real numbers
$\mathbb{R}^+$	Set of non-negative real numbers
$\delta(\cdot)$	Dirac delta distribution
$f'(\cdot)$	Ordinary derivative of $f(\cdot)$
$\dot{f}(\cdot)$	Ordinary derivative of $f(\cdot)$ with respect to *time*
$\partial_x f$	Partial derivative of f with respect to x
$\sup_{\mathcal{I}} \mathcal{S}$	Supremum of $\mathcal{S}$ on the interval $\mathcal{I}$
$L_2(\mathcal{I})$	The space of functions $u(x,t), u : \mathcal{I} \times \mathbb{R}^+ \to \mathbb{R}$ whose spatial $L_2(\mathcal{I})$ norm defined by $\|u(t)\| = \left(\int_{\mathcal{I}} u^2(x,t)dx\right)^{1/2}$ is finite
$\mathcal{L}_p$	The space of time functions $f : \mathbb{R}^+ \to \mathbb{R}$ whose p-norm defined by $\|f\|_p = \left(\int_0^\infty \|f(t)|^p dt\right)^{1/p}$ for $p \in [1, \infty)$ is finite
$\mathcal{L}_\infty$	The space of time functions $f : \mathbb{R}^+ \to \mathbb{R}$ whose infinity norm defined by $\|f\|_\infty = \sup_{t \geq 0} \|f(t)\|$ is finite

- Compared with recent results on the adaptive control of a 2×2 coupled hyperbolic PDE cascaded with an ODE through the boundary [27], [28], this paper solves a more challenging problem in which the ODE is connected not at the boundary, but rather, at an interior point of a 2×2 system of coupled hyperbolic PDE via a Dirac delta distribution. In fact, the Rijke tube model falls into a special class of the so-called sandwich systems [36]. Moreover, we consider the situation in which the unknown parameters exist at the state and the input coefficients of the ODE.

D. ORGANIZATION

The remainder of this paper is organized as follows: Section II presents the adaptive control problem under consideration and Section III reviews the non-adaptive scheme. The proposed adaptive scheme is discussed in Section IV, and the stability analysis of the closed-loop system is investigated in Section V. Simulation studies are then presented in Section VI and conclusions are provided in Section VII.

E. NOTATION

Table 1 shows the notations adopted in this paper.

II. PROBLEM STATEMENT

The linearized ODE-PDE model of thermoacoustic oscillations in the Rijke tube system is described by [2]

$$\begin{aligned}
&\partial_t v(x,t) + \frac{1}{\bar{\rho}} \partial_x P(x,t) = 0, \\
&\partial_t P(x,t) + \gamma \bar{P} \partial_x v(x,t) = \frac{\gamma - 1}{A} \delta(x - x_0) Q(t), \\
&\tau \dot{Q}(t) = -Q(t) + f'(\bar{v})(T_w - \bar{T}_{gas}) v(x_0,t),
\end{aligned} \tag{1}$$

with the boundary conditions

$$P(0,t) = U(t), \quad P(l,t) = Z_L v(l,t), \tag{2}$$

where $(x,t) \in [0,l] \times \mathbb{R}^+$ and $f(v) = l_w(\kappa + \kappa_v\sqrt{|v|})$. The parameters of the model (1)-(2) are given in Table 2. The PDE states $v(x,t)$ and $P(x,t)$ represent the fluctuations of acoustic velocity and pressure along the tube, respectively. The ODE state $Q(t)$ represents the heat power release by the coil located at $x_0 \in (0, l/2)$. This ODE state is connected to the PDE states via the Dirac delta distribution, δ.

The Rijke tube model (1)-(2) can be reformulated through applying the Riemann coordinates [11]

$$\begin{aligned} P(x,t) &= \frac{1}{2}\big(R_1(x,t) + R_2(x,t)\big), \\ v(x,t) &= \frac{1}{2\sqrt{\gamma \bar{P}\bar{\rho}}}\big(R_1(x,t) - R_2(x,t)\big), \end{aligned} \tag{3}$$

into a 2×2 transport PDEs convecting in opposite directions with a point source term

$$\begin{aligned} &\partial_t R_1(x,t) + \lambda \partial_x R_1(x,t) = \frac{\gamma - 1}{A}\delta(x - x_0)Q(t), \\ &\partial_t R_2(x,t) - \lambda \partial_x R_2(x,t) = \frac{\gamma - 1}{A}\delta(x - x_0)Q(t), \\ &\dot{Q}(t) = -\zeta Q(t) + c\big(R_1(x_0,t) - R_2(x_0,t)\big), \end{aligned} \tag{4}$$

with the boundary conditions

$$R_1(0,t) = -R_2(0,t) + 2U(t), \quad R_2(l,t) = \alpha R_1(l,t), \tag{5}$$

where $\zeta = 1/\tau$, $c = \frac{f'(\bar{v})(T_w - \bar{T}_{gas})}{2\tau\sqrt{\gamma \bar{P}\bar{\rho}}}$, $\lambda = \sqrt{\gamma \frac{\bar{P}}{\bar{\rho}}}$ and $\alpha = \frac{Z_L - \bar{\rho}\lambda}{Z_L + \bar{\rho}\lambda}$. Assuming that the parameters of the model are known, a full state feedback boundary controller has been developed in [5].

From a practical standpoint, there are uncertain parameters in the mathematical model of the system; these include the unknown heat release time constant, τ, unknown steady-state velocity, $\bar{v}$, and unknown wire temperature, T_w [5]. The uncertainty in these parameters leads to the unknown coefficients, ζ and c, of the ODE system (4). The goal is to develop an adaptive control law $U(t)$ that stabilizes the system (4)-(5) in which ζ and c are treated as unknown parameters and can be estimated by an adaptive mechanism.

The uncertain parameters τ, $\bar{v}$ and T_w in the ODE system of (1) are assumed to belong to some intervals. Therefore, we consider the following assumption for the coefficients ζ and c in the ODE system of (4).

Assumption 1: There exist positive and known constants $\underline{\zeta}$, $\bar{\zeta}$ and $\underline{c}$, $\bar{c}$ such that $\zeta \in [\underline{\zeta}, \bar{\zeta}]$ and $c \in [\underline{c}, \bar{c}]$.

III. OVERVIEW OF THE NON-ADAPTIVE SCHEME

The proposed adaptive stabilization scheme builds upon a recent effort [5] which considered the boundary stabilization of (4)-(5) when all parameters of the model are known. As a foundation for our work, in this section, we briefly review the design procedure of the non-adaptive scheme of [5].

TABLE 2. The parameters of the Rijke tube model (1)-(2).

Description	Symbol
Steady-state pressure	$\bar{P}$
Steady-state velocity	$\bar{v}$
Steady-state density	$\bar{\rho}$
Steady-state gas temperature	$\bar{T}_{gas}$
Fluid thermal conductivity	κ
Empirical constant	κ_v
Reflection loss	Z_L
Length of the tube	l
Tube cross-section	A
Heater coil position	x_0
Heat capacity ratio	γ
Heat release time constant	τ
Wire temperature	T_w
Wire length	l_w

At first, the spatial domain of the system is folded at the discontinuity point, x_0, raised by the Dirac delta distribution. Specifically, by introducing the folding transformation

$$z = \begin{cases} \dfrac{x}{x_0}, & x \in [0, x_0] \\ \dfrac{l - x}{l - x_0}, & x \in [x_0, l] \end{cases} \tag{6}$$

along with the new state variables

$$\begin{aligned} R_{11}(x,t) &= R_1(x,t), \quad x \in [0, x_0] \\ R_{12}(x,t) &= R_2(x,t), \quad x \in [0, x_0] \\ R_{21}(x,t) &= R_1(x,t), \quad x \in [x_0, l] \\ R_{22}(x,t) &= R_2(x,t), \quad x \in [x_0, l] \end{aligned} \tag{7}$$

the Rijke tube model (4)-(5) is reformulated as

$$\begin{aligned} &\partial_t R_{11}(z,t) + \lambda_1 \partial_z R_{11}(z,t) = 0, \\ &\partial_t R_{12}(z,t) - \lambda_1 \partial_z R_{12}(z,t) = 0, \\ &\partial_t R_{21}(z,t) - \lambda_2 \partial_z R_{21}(z,t) = 0, \\ &\partial_t R_{22}(z,t) + \lambda_2 \partial_z R_{22}(z,t) = 0, \\ &\dot{Q}(t) = -\zeta Q(t) + c\big(R_{11}(1,t) - R_{22}(1,t)\big), \end{aligned} \tag{8}$$

with the boundary conditions

$$\begin{aligned} R_{11}(0,t) &= -R_{12}(0,t) + 2U(t), \\ R_{12}(1,t) &= R_{22}(1,t) + c_1 Q(t), \\ R_{21}(1,t) &= R_{11}(1,t) + c_1 Q(t), \\ R_{22}(0,t) &= \alpha R_{21}(0,t), \end{aligned} \tag{9}$$

where $c_1 = \frac{\gamma - 1}{\lambda A}$, $\lambda_1 = \frac{\lambda}{x_0}$ and $\lambda_2 = \frac{\lambda}{l - x_0}$.

As the next step, the infinite-dimensional backstepping method is used to determine the control law. The basic idea of this method is to use an invertible integral transformation with bounded kernels along with a control law to transform the original system into the so-called target system with desirable stability properties. For this purpose, the stable target system

is chosen as

$$\begin{aligned}
&\partial_t \mathcal{S}_{11}(z,t) + \lambda_1 \partial_z \mathcal{S}_{11}(z,t) = 0,\\
&\partial_t R_{12}(z,t) - \lambda_1 \partial_z R_{12}(z,t) = 0,\\
&\partial_t R_{21}(z,t) - \lambda_2 \partial_z R_{21}(z,t) = 0,\\
&\partial_t R_{22}(z,t) + \lambda_2 \partial_z R_{22}(z,t) = 0,\\
&\dot{Q}(t) = -\big(\zeta + c_1 c\big) Q(t) + c\big(\mathcal{S}_{11}(1,t) - R_{22}(1,t)\big),
\end{aligned} \tag{10}$$

with the boundary conditions

$$\begin{aligned}
&\mathcal{S}_{11}(0,t) = 0,\\
&R_{12}(1,t) = R_{22}(1,t) + c_1 Q(t),\\
&R_{21}(1,t) = \mathcal{S}_{11}(1,t),\\
&R_{22}(0,t) = \alpha R_{21}(0,t).
\end{aligned} \tag{11}$$

This target system has a cascade structure and the boundary condition $\mathcal{S}_{11}(0,t) = 0$ has a crucial role in the stability of the system. Notice in particular that the unforced transport PDE for $\mathcal{S}_{11}(z,t)$ drives the transport PDE for $R_{21}(z,t)$, which subsequently drives the transport PDE for $R_{22}(z,t)$. Therefore, $\mathcal{S}_{11}(z,t) = 0,\ \forall t \geq \lambda_1^{-1}$, and then $R_{21}(z,t) = 0,\ \forall t \geq \lambda_1^{-1} + \lambda_2^{-1}$, and subsequently $R_{22}(z,t) = 0,\ \forall t \geq \lambda_1^{-1} + 2\lambda_2^{-1}$. For $t \geq \lambda_1^{-1} + 2\lambda_2^{-1}$, we have $\dot{Q}(t) = -\big(\zeta + c_1 c\big)Q(t)$ and $R_{12}(1,t) = c_1 Q(t)$. Therefore, $Q(t)$, and then, $R_{12}(z,t)$ approaches zero.

In order to map (8)-(9) into (10)-(11), the invertible backstepping transformation is introduced as

$$\begin{aligned}
\mathcal{S}_{11}(z,t) = R_{11}(z,t) &- \int_z^1 K(z,\xi) R_{11}(\xi,t) d\xi\\
&- \int_0^1 G(z,\xi) R_{22}(\xi,t) d\xi - \varphi(z) Q(t),
\end{aligned} \tag{12}$$

where $K(z,\xi)$ is the kernel of a Volterra-type integral transformation defined on

$$\mathcal{T}_0 = \big\{(z,\xi) \in \mathbb{R} \times \mathbb{R} \mid\ 0 \leqslant z \leqslant \xi \leqslant 1\big\}, \tag{13}$$

and $G(z,\xi)$ is the kernel of a Fredholm-type integral transformation defined on

$$\mathcal{T}_1 = \big\{(z,\xi) \in \mathbb{R} \times \mathbb{R} \mid\ 0 \leqslant \xi \leqslant 1,\ \ 0 \leqslant z \leqslant 1\big\}. \tag{14}$$

By matching the system (8)-(9) and the target system (10)-(11), the kernel equations are obtained as

$$\begin{aligned}
&\partial_\xi K(z,\xi) + \partial_z K(z,\xi) = 0,\\
&\partial_\xi G(z,\xi) + \frac{\lambda_1}{\lambda_2} \partial_z G(z,\xi) = 0,\\
&\lambda_1 \partial_z \varphi(z) - \zeta \varphi(z) = 0,\\
&\lambda_1 K(z,1) - c\varphi(z) = 0,\\
&\lambda_2 G(z,1) + c\varphi(z) = 0,\\
&G(z,0) = 0.
\end{aligned} \tag{15}$$

The well-posedness of (15) is shown in [5], and the explicit solutions of the kernels are obtained as

$$\begin{aligned}
&\varphi(z) = -c_1 e^{\frac{(z-1)\zeta}{\lambda_1}},\ z \in [0,1]\\
&K(z,\xi) = \frac{c}{\lambda_1} \varphi(z - \xi + 1),\\
&G(z,\xi) = \begin{cases} 0, & \xi \leqslant 1 + \dfrac{\lambda_2}{\lambda_1}(z-1)\\ -\dfrac{c}{\lambda_2} \varphi\big(z - \dfrac{\lambda_1}{\lambda_2}(\xi - 1)\big), & \xi > 1 + \dfrac{\lambda_2}{\lambda_1}(z-1) \end{cases}
\end{aligned} \tag{16}$$

The state feedback control law is obtained by substituting the boundary conditions $\mathcal{S}_{11}(0,t) = 0$ and $R_{11}(0,t) = -R_{12}(0,t) + 2U(t)$ into (12) as [5]

$$\begin{aligned}
U(t) = \frac{1}{2}\Big(&R_{12}(0,t) + \int_0^1 K(0,\xi) R_{11}(\xi,t) d\xi\\
&+ \int_0^1 G(0,\xi) R_{22}(\xi,t) d\xi + \varphi(0) Q(t)\Big).
\end{aligned} \tag{17}$$

Experimentally, the control law (17) can not be used for the boundary stabilization of thermoacoustic oscillations in the Rijke tube due to the requirement of full state measurement [5]. Therefore, a full state observer for the Rijke tube using a single boundary acoustic pressure sensor has been presented in [37].

In what follows, we develop an adaptive control law using a few measurements of states, while the coefficients of the first-order ODE in (4) are unknown.

IV. PROPOSED ADAPTIVE SCHEME

In this section, an adaptive control scheme is proposed for the stabilization of thermoacoustic instability in the Rijke tube model (4)-(5) with the unknown parameters ζ and c. The proposed adaptive scheme is formed by combining an online parameter estimator with a control law inspired by the known parameter case.

A. UPDATE LAWS

In this section, we consider the design of the adaptive laws for online estimation of the unknown parameters. Consider the heat release dynamics in the Rijke tube model described by

$$\dot{Q}(t) = -\zeta Q(t) + c\big(R_{11}(1,t) - R_{22}(1,t)\big), \tag{18}$$

where ζ and c are the unknown parameters to be estimated. To develop the estimator, we first convert the dynamical model (18) into the static parametric model where the unknown parameters appear in a linear form and then we use the standard gradient algorithm. By taking the Laplace transform on both sides of (18), ignoring the initial conditions, we have

$$sQ(s) = -\zeta Q(s) + c\big(R_{11}(1,s) - R_{22}(1,s)\big), \tag{19}$$

where s denotes the Laplace variable. Let γ_1 be a positive real number, then

$$(s+\gamma_1)Q(s) = \big(\gamma_1 - \zeta\big)Q(s) + c\Big(R_{11}(1,s) - R_{22}(1,s)\Big), \tag{20}$$

which is equivalent to

$$Q(s) = \big(\gamma_1 - \zeta\big)\frac{Q(s)}{s+\gamma_1} + c\frac{R_{11}(1,s) - R_{22}(1,s)}{s+\gamma_1}. \tag{21}$$

Define

$$\begin{aligned} q(s) &= \frac{Q(s)}{s+\gamma_1}, \\ r(s) &= \frac{R_{11}(1,s) - R_{22}(1,s)}{s+\gamma_1}, \end{aligned} \tag{22}$$

or, in the time domain

$$\begin{aligned} \dot{q}(t) &= -\gamma_1 q(t) + Q(t), \\ \dot{r}(t) &= -\gamma_1 r(t) + \Big(R_{11}(1,t) - R_{22}(1,t)\Big). \end{aligned} \tag{23}$$

Then, we can represent (21) in the time domain as

$$Q(t) = (\gamma_1 - \zeta)q(t) + cr(t) + \epsilon(t), \tag{24}$$

where $\epsilon(t)$ is due to the initial conditions. According to Lemma 1 of Appendix A, $\epsilon(t)$ is an exponentially decaying signal. Using $\hat{\zeta}(t)$ and $\hat{c}(t)$ as the estimates of ζ and c, respectively, in analogy with (24), we generate the estimated value $\hat{Q}(t)$ of $Q(t)$ as

$$\hat{Q}(t) = \big(\gamma_1 - \hat{\zeta}(t)\big)q(t) + \hat{c}(t)r(t). \tag{25}$$

We also define the parameter estimation errors as

$$\tilde{\zeta}(t) = \zeta - \hat{\zeta}(t), \quad \tilde{c}(t) = c - \hat{c}(t), \tag{26}$$

and the identifier error as

$$\begin{aligned} \tilde{Q}(t) &= Q(t) - \hat{Q}(t), \\ &= Q(t) + \big(\hat{\zeta}(t) - \gamma_1\big)q(t) - \hat{c}(t)r(t) + \epsilon(t). \end{aligned} \tag{27}$$

Now, using the normalized gradient algorithm with projection [39], the update laws of the ODE coefficients are derived as follows

$$\begin{aligned} \dot{\hat{\zeta}}(t) &= \mathrm{Proj}_{[\underline{\zeta},\bar{\zeta}]}\big(\hat{\zeta}(t), \tau_\zeta(t)\big), \\ \dot{\hat{c}}(t) &= \mathrm{Proj}_{[\underline{c},\bar{c}]}\big(\hat{c}(t), \tau_c(t)\big), \\ \tau_\zeta(t) &= -\mu_1 \frac{\tilde{Q}(t)q(t)}{1+q^2(t)+r^2(t)}, \\ \tau_c(t) &= \mu_2 \frac{\tilde{Q}(t)r(t)}{1+q^2(t)+r^2(t)}, \end{aligned} \tag{28}$$

where the positive constants μ_1 and μ_2 are the adaptation gains and the standard projection operator is defined in the following way

$$\mathrm{Proj}_{[\underline{\zeta},\bar{\zeta}]}\big(\hat{\zeta}(t), \tau_\zeta(t)\big) = \tau_\zeta(t)\begin{cases} 0 & \hat{\zeta}(t) = \underline{\zeta},\ \tau_\zeta(t) \leqslant 0 \\ 0 & \hat{\zeta}(t) = \bar{\zeta},\ \tau_\zeta(t) > 0 \\ 1 & \text{otherwise.} \end{cases} \tag{29}$$

The other operator $\mathrm{Proj}_{[\underline{c},\bar{c}]}\big(\hat{c}(t), \tau_c(t)\big)$ is defined similar to the operator (29), both of which are used to keep the parameter estimates in the intervals of Assumption 1. According to Theorem 2.4.2 in [39], the identifier (25) with filters (23), and the update laws (28) with the initial conditions $\hat{\zeta}(0) \in [\underline{\zeta}, \bar{\zeta}]$ and $\hat{c}(0) \in [\underline{c}, \bar{c}]$ satisfy the following properties

$$\begin{aligned} &\tilde{\zeta}(t), \tilde{c}(t) \in \mathcal{L}_\infty, \\ &\frac{\tilde{Q}(t)}{\sqrt{1+q^2(t)+r^2(t)}} \in \mathcal{L}_2 \cap \mathcal{L}_\infty, \\ &\dot{\hat{\zeta}}(t), \dot{\hat{c}}(t) \in \mathcal{L}_2 \cap \mathcal{L}_\infty. \end{aligned} \tag{30}$$

B. CONTROL LAW

The proposed adaptive controller is obtained by substituting the estimation of unknown parameters, i.e., $\hat{\zeta}(t)$ and $\hat{c}(t)$, and the identifier output $\hat{Q}(t)$ into the control law (17), as follows

$$\begin{aligned} U(t) = \frac{1}{2}\Bigg(&R_{12}(0,t) + \int_0^1 \hat{K}(0,\xi,t)R_{11}(\xi,t)d\xi \\ &+ \int_0^1 \hat{G}(0,\xi,t)R_{22}(\xi,t)d\xi + \hat{\varphi}(0,t)\hat{Q}(t)\Bigg), \end{aligned} \tag{31}$$

where

$$\begin{aligned} \hat{\varphi}(z,t) &= -c_1 e^{\frac{(z-1)\hat{\zeta}(t)}{\lambda_1}}, \\ \hat{K}(z,\xi,t) &= \frac{\hat{c}(t)}{\lambda_1}\hat{\varphi}(z-\xi+1,t), \\ \hat{G}(z,\xi,t) &= \begin{cases} 0, & \\ & \xi \leqslant 1 + \dfrac{\lambda_2}{\lambda_1}(z-1) \\ -\dfrac{\hat{c}(t)}{\lambda_2}\hat{\varphi}\big(z - \dfrac{\lambda_1}{\lambda_2}(\xi-1), t\big), & \\ & \xi > 1 + \dfrac{\lambda_2}{\lambda_1}(z-1) \end{cases} \end{aligned} \tag{32}$$

In the sequel, the control law (31) is revisited such that it does not require the measurement of the entire distributed states $R_{11}(z,t)$ and $R_{22}(z,t)$. To this end, from the transport PDEs

$$\begin{aligned} \partial_t R_{11}(z,t) + \lambda_1 \partial_z R_{11}(z,t) &= 0, \\ \partial_t R_{22}(z,t) + \lambda_2 \partial_z R_{22}(z,t) &= 0, \end{aligned} \tag{33}$$

we have

$$R_{11}(z,t) = R_{11}(0, t - \frac{z}{\lambda_1}), \tag{34}$$

$$R_{22}(z,t) = R_{22}(0, t - \frac{z}{\lambda_2}). \tag{35}$$

Moreover, from (7), we have

$$\begin{aligned} R_{11}(0, t - \frac{z}{\lambda_1}) &= R_1(0, t - \frac{z}{\lambda_1}), \\ R_{22}(0, t - \frac{z}{\lambda_2}) &= R_2(l, t - \frac{z}{\lambda_2}), \end{aligned} \tag{36}$$

and

$$R_{12}(0,t) = R_2(0,t). \tag{37}$$

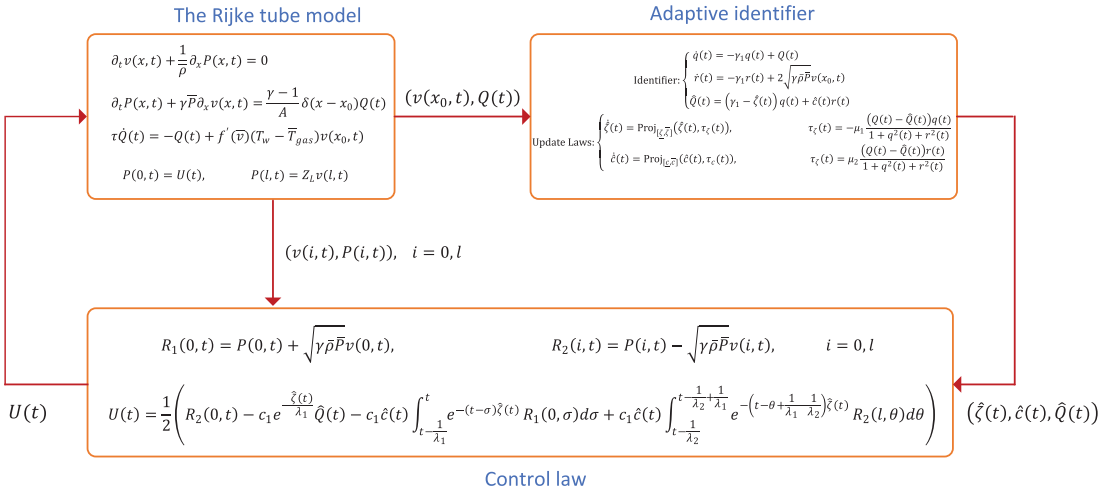

FIGURE 3. Proposed scheme for adaptive stabilization of the ODE-PDE Rijke tube model. The model parameters are given in Table 2, and $\lambda_1=\frac{\lambda}{x_0}$, $\lambda_2=\frac{\lambda}{l-x_0}$ and $\lambda=\sqrt{\frac{\gamma\bar P}{\bar\rho}}$.

Therefore, the control law (31) can be rewritten as

$$U(t)=\frac{1}{2}\Big(R_2(0,t)+\int_0^1\hat K(0,\xi,t)R_1(0,t-\frac{\xi}{\lambda_1})d\xi+\int_0^1\hat G(0,\xi,t)R_2(l,t-\frac{\xi}{\lambda_2})d\xi+\hat\varphi(0,t)\hat Q(t)\Big). \tag{38}$$

By substituting the kernels (32), and using the change of variables $\sigma=t-\frac{\xi}{\lambda_1}$ and $\theta=t-\frac{\xi}{\lambda_2}$, we arrive at

$$U(t)=\frac{1}{2}\Big(R_2(0,t)-c_1e^{-\frac{\hat\zeta(t)}{\lambda_1}}\hat Q(t)-c_1\hat c(t)\int_{t-\frac{1}{\lambda_1}}^{t}e^{-(t-\sigma)\hat\zeta(t)}R_1(0,\sigma)d\sigma+c_1\hat c(t)\int_{t-\frac{1}{\lambda_2}}^{t-\frac{1}{\lambda_2}+\frac{1}{\lambda_1}}e^{-(t-\theta+\frac{1}{\lambda_1}-\frac{1}{\lambda_2})\hat\zeta(t)}R_2(l,\theta)d\theta\Big), \tag{39}$$

where $\hat Q(t)$ is given by (25), and from (23), (7) and (3), we have

$$\begin{aligned}\dot q(t)&=-\gamma_1 q(t)+Q(t),\\ \dot r(t)&=-\gamma_1 r(t)+\big(R_1(x_0,t)-R_2(x_0,t)\big)\\ &=-\gamma_1 r(t)+2\sqrt{\gamma\bar\rho\bar P}v(x_0,t).\end{aligned} \tag{40}$$

The block diagram of the proposed scheme for the adaptive stabilization of the ODE-PDE Rijke tube model system is depicted in Fig. 3. Note that, we use (3) to express $R_1(0,t)$, $R_2(0,t)$, and $R_2(l,t)$ in terms of $\big(v(i,t),P(i,t)\big)$, $i=0,l$ as

$$\begin{aligned}R_1(0,t)&=P(0,t)+\sqrt{\gamma\bar\rho\bar P}v(0,t),\\ R_2(i,t)&=P(i,t)-\sqrt{\gamma\bar\rho\bar P}v(i,t),\ i=0,l\end{aligned} \tag{41}$$

It can be seen that the proposed scheme requires only the measurements of $P(0,t)$, $P(l,t)$, $v(0,t)$, $v(l,t)$, $v(x_0,t)$ and $Q(t)$, rather than the entire distributed states of the system.

V. STABILITY ANALYSIS

Theorem 1: Consider the closed-loop system consisting of the plant (4)-(5), identifier (25) and (40), update laws (28) and the control law (39). Let Assumption 1 hold and the initial conditions satisfy $\big(R_1(x,0),R_2(x,0)\big)\in L_2([0,l])\times L_2([0,l])$, $Q(0)\in\mathbb{R}$, $\hat\zeta(0)\in[\underline\zeta,\bar\zeta]$ and $\hat c(0)\in[\underline c,\bar c]$. Then

$$\begin{aligned}&\|R_i(t)\|,Q(t),q(t),r(t)\in\mathcal{L}_2\cap\mathcal{L}_\infty,\ i=1,2\\ &\lim_{t\to\infty}\|R_i(t)\|=0,\\ &\lim_{t\to\infty}Q(t)=0,\quad\lim_{t\to\infty}\hat Q(t)=0,\\ &\lim_{t\to\infty}q(t)=0,\quad\lim_{t\to\infty}r(t)=0.\end{aligned} \tag{42}$$

Proof: We consider the dynamical system governing $\big(R_1(x,t),R_2(x,t),\hat Q(t),q(t),r(t)\big)$ and establish the boundedness and regulation results stated in Theorem 1 for $\|R_1(t)\|$, $\|R_2(t)\|$, $\hat Q(t)$, $q(t)$, $r(t)$. The boundedness and regulation of $Q(t)$ can then follow from (24). The proof is carried out using the following four steps.

Step 1: System equations and folding transformation: In this step, we derive the governing equations of the system $\big(R_1(x,t),R_2(x,t),\hat Q(t),q(t),r(t)\big)$, and use the folding transformation to translate the discontinuity point of the system to the boundary conditions. From (25) and (40), we have

$$\begin{aligned}\dot{\hat Q}(t)&=-\dot{\hat\zeta}(t)q(t)+\dot{\hat c}(t)r(t)\\ &\quad+\big(\gamma_1-\hat\zeta(t)\big)\big(-\gamma_1q(t)+Q(t)\big)\\ &\quad+\hat c(t)\Big(-\gamma_1r(t)+\big(R_1(x_0,t)-R_2(x_0,t)\big)\Big)\\ &=-\dot{\hat\zeta}(t)q(t)+\dot{\hat c}(t)r(t)+\big(\gamma_1-\hat\zeta(t)\big)\underbrace{Q(t)}_{\hat Q(t)+\tilde Q(t)}\\ &\quad-\gamma_1\Big(\underbrace{\big(\gamma_1-\hat\zeta(t)\big)q(t)+\hat c(t)r(t)}_{\hat Q(t)}\Big)\\ &\quad+\hat c(t)\Big(R_1(x_0,t)-R_2(x_0,t)\Big)\end{aligned}$$

$$= -\dot{\hat{\zeta}}(t)q(t) + \dot{\hat{c}}(t)r(t) + \big(\gamma_1 - \hat{\zeta}(t)\big)\tilde{Q}(t) - \hat{\zeta}(t)\hat{Q}(t) + \hat{c}(t)\big(R_1(x_0,t) - R_2(x_0,t)\big). \quad (43)$$

Therefore, the $\big(R_1(x,t), R_2(x,t), \hat{Q}(t), q(t), r(t)\big)$-system is governed by

$$\begin{aligned}
&\partial_t R_1(x,t) + \lambda\partial_x R_1(x,t) = \frac{\gamma-1}{A}\delta(x-x_0)\hat{Q}(t),\\
&\partial_t R_2(x,t) - \lambda\partial_x R_2(x,t) = \frac{\gamma-1}{A}\delta(x-x_0)\hat{Q}(t),\\
&\dot{\hat{Q}}(t) = -\hat{\zeta}(t)\hat{Q}(t) + \hat{c}(t)\big(R_1(x_0,t) - R_2(x_0,t)\big)\\
&\qquad - \dot{\hat{\zeta}}(t)q(t) + \dot{\hat{c}}(t)r(t) + \big(\gamma_1 - \hat{\zeta}(t)\big)\tilde{Q}(t),\\
&\dot{q}(t) = -\gamma_1 q(t) + \hat{Q}(t) + \tilde{Q}(t),\\
&\dot{r}(t) = -\gamma_1 r(t) + \big(R_1(x_0,t) - R_2(x_0,t)\big),
\end{aligned} \quad (44)$$

with the boundary conditions

$$\begin{aligned}
R_1(0,t) &= -R_2(0,t) + 2U(t),\\
R_2(l,t) &= \alpha R_1(l,t),
\end{aligned} \quad (45)$$

where the control law $U(t)$ is given by (39).

Now, we use the folding transformation (6) along with the state variables (7) and rewrite (44)-(45) as

$$\begin{aligned}
&\partial_t R_{11}(z,t) + \lambda_1\partial_z R_{11}(z,t) = 0,\\
&\partial_t R_{12}(z,t) - \lambda_1\partial_z R_{12}(z,t) = 0,\\
&\partial_t R_{21}(z,t) - \lambda_2\partial_z R_{21}(z,t) = 0,\\
&\partial_t R_{22}(z,t) + \lambda_2\partial_z R_{22}(z,t) = 0,\\
&\dot{\hat{Q}}(t) = -\hat{\zeta}(t)\hat{Q}(t) + \hat{c}(t)\big(R_{11}(1,t) - R_{22}(1,t)\big)\\
&\qquad - \dot{\hat{\zeta}}(t)q(t) + \dot{\hat{c}}(t)r(t) + \big(\gamma_1 - \hat{\zeta}(t)\big)\tilde{Q}(t),\\
&\dot{q}(t) = -\gamma_1 q(t) + \hat{Q}(t) + \tilde{Q}(t),\\
&\dot{r}(t) = -\gamma_1 r(t) + \big(R_{11}(1,t) - R_{22}(1,t)\big),
\end{aligned} \quad (46)$$

with the boundary conditions

$$\begin{aligned}
R_{11}(0,t) &= -R_{12}(0,t) + 2U(t),\\
R_{12}(1,t) &= R_{22}(1,t) + c_1\hat{Q}(t) + c_1\tilde{Q}(t),\\
R_{21}(1,t) &= R_{11}(1,t) + c_1\hat{Q}(t) + c_1\tilde{Q}(t),\\
R_{22}(0,t) &= \alpha R_{21}(0,t),
\end{aligned} \quad (47)$$

where the control law $U(t)$ is given by (31).

Step 2: Backstepping transformation and target system: In this step, we propose an infinite-dimensional backstepping transformation that converts the system (46)-(47) along with the control law (31) into the new system called the target system, which is more convenient for stability analysis. The backstepping transformation is invertible, enabling the establishment of the norm equivalence between the target system and the original system.

Consider the infinite-dimensional backstepping transformation

$$S_{11}(z,t) = R_{11}(z,t) - \int_z^1 \hat{K}(z,\xi,t)R_{11}(\xi,t)d\xi - \int_0^1 \hat{G}(z,\xi,t)R_{22}(\xi,t)d\xi - \hat{\varphi}(z,t)\hat{Q}(t), \quad (48)$$

where the kernels $\hat{K}(z,\xi,t)$, $\hat{G}(z,\xi,t)$ and $\hat{\varphi}(z,t)$ satisfy

$$\begin{aligned}
\partial_\xi\hat{K}(z,\xi,t) + \partial_z\hat{K}(z,\xi,t) &= 0,\\
\partial_\xi\hat{G}(z,\xi,t) + \frac{\lambda_1}{\lambda_2}\partial_z\hat{G}(z,\xi,t) &= 0,\\
\lambda_1\partial_z\hat{\varphi}(z,t) - \hat{\zeta}(t)\hat{\varphi}(z,t) &= 0,\\
\lambda_1\hat{K}(z,1,t) - \hat{c}(t)\hat{\varphi}(z,t) &= 0,\\
\lambda_2\hat{G}(z,1,t) + \hat{c}(t)\hat{\varphi}(z,t) &= 0,\\
\hat{G}(z,0,t) &= 0.
\end{aligned} \quad (49)$$

The transformation (48) and the kernel equations (49) are adaptive versions of (12) and (15), respectively, where the unknown parameters ζ and c are replaced by the adaptive identifier estimates $\hat{\zeta}(t)$ and $\hat{c}(t)$, and the ODE state $Q(t)$ is replaced by the adaptive identifier output $\hat{Q}(t)$. Similar to (15), the kernel equations (49) are well-posed and by replacing ζ and c with $\hat{\zeta}(t)$ and $\hat{c}(t)$ in (16) the explicit solutions of the kernels are obtained as (32). The inverse transformation of (48) is [38]

$$R_{11}(z,t) = S_{11}(z,t) + \int_z^1 N(z,\xi,t)S_{11}(\xi,t)d\xi + \chi(z,t), \quad (50)$$

where

$$\begin{aligned}
\chi(z,t) &= \Psi(z,t) + \int_z^1 N(z,\xi,t)\Psi(\xi,t)d\xi,\\
\Psi(z,t) &= \hat{\varphi}(z,t)\hat{Q}(t) + \int_0^1 \hat{G}(z,\xi,t)R_{22}(\xi,t)d\xi,\\
N(z,\xi,t) &= \hat{K}(z,\xi,t) + \int_z^\xi \hat{K}(z,\sigma,t)N(\sigma,\xi,t)d\sigma.
\end{aligned} \quad (51)$$

As shown in Lemma 2 of Appendix A, the backstepping transformation (48) maps the system (46)-(47) along with the control law (31) into the target system

$$\begin{aligned}
&\partial_t S_{11}(z,t) + \lambda_1\partial_z S_{11}(z,t)\\
&= -\int_z^1 \partial_t\hat{K}(z,\xi,t)R_{11}(\xi,t)d\xi\\
&\quad - \int_0^1 \partial_t\hat{G}(z,\xi,t)R_{22}(\xi,t)d\xi - \partial_t\hat{\varphi}(z,t)\hat{Q}(t)\\
&\quad + \dot{\hat{\zeta}}(t)\hat{\varphi}(z,t)q(t) - \dot{\hat{c}}(t)\hat{\varphi}(z,t)r(t)\\
&\quad - \big(\gamma_1 - \hat{\zeta}(t)\big)\hat{\varphi}(z,t)\tilde{Q}(t),\\
&\partial_t R_{12}(z,t) - \lambda_1\partial_z R_{12}(z,t) = 0,\\
&\partial_t R_{21}(z,t) - \lambda_2\partial_z R_{21}(z,t) = 0,\\
&\partial_t R_{22}(z,t) + \lambda_2\partial_z R_{22}(z,t) = 0,\\
&\dot{\hat{Q}}(t) = -\Big(\hat{\zeta}(t) + c_1\hat{c}(t)\Big)\hat{Q}(t) + \hat{c}(t)\Big(S_{11}(1,t) - R_{22}(1,t)\Big)\\
&\qquad - \dot{\hat{\zeta}}(t)q(t) + \dot{\hat{c}}(t)r(t) + \Big(\gamma_1 - \hat{\zeta}(t)\Big)\tilde{Q}(t),
\end{aligned}$$

$$\begin{aligned}&\dot{q}(t)\\&= -\gamma_1 q(t) + \hat{Q}(t) + \tilde{Q}(t),\\&\dot{r}(t)\\&= -\gamma_1 r(t) - c_1\hat{Q}(t) + \Big(S_{11}(1,t) - R_{22}(1,t)\Big),\end{aligned} \tag{52}$$

with the boundary conditions

$$\begin{aligned}&S_{11}(0,t) = 0,\\&R_{12}(1,t) = R_{22}(1,t) + c_1\hat{Q}(t) + c_1\tilde{Q}(t),\\&R_{21}(1,t) = S_{11}(1,t) + c_1\tilde{Q}(t),\\&R_{22}(0,t) = \alpha R_{21}(0,t).\end{aligned} \tag{53}$$

Step 3: Boundedness and regulation of the target system: In this step, we establish the boundedness and regulation of the target system (52)-(53). In other words, we prove

$$\begin{aligned}&\|S_{11}(t)\|, \|R_{12}(t)\|, \|R_{21}(t)\|, \|R_{22}(t)\| \in \mathcal{L}_2 \cap \mathcal{L}_\infty,\\&\hat{Q}(t), q(t), r(t) \in \mathcal{L}_2 \cap \mathcal{L}_\infty,\end{aligned} \tag{54}$$

and

$$\begin{aligned}&\lim_{t\to\infty} \|S_{11}(t)\| = 0, \quad \lim_{t\to\infty} \|R_{12}(t)\| = 0,\\&\lim_{t\to\infty} \|R_{21}(t)\| = 0, \quad \lim_{t\to\infty} \|R_{22}(t)\| = 0,\\&\lim_{t\to\infty} \hat{Q}(t) = 0, \quad \lim_{t\to\infty} q(t) = 0, \quad \lim_{t\to\infty} r(t) = 0.\end{aligned} \tag{55}$$

The main idea is to consider a Lyapunov function candidate and show that it satisfies the differential inequality (A27). The boundedness and regulation results (54) and (55) can then follow from Lemma 5 of Appendix A.

To begin with, consider the Lyapunov functional

$$\begin{aligned}V(t) = {} & b_1\int_0^1 e^{-z}S_{11}^2(z,t)dz + \int_0^1 e^{z}R_{12}^2(z,t)dz\\&+ b_2\int_0^1 e^{z}R_{21}^2(z,t)dz + b_3\int_0^1 e^{-z}R_{22}^2(z,t)dz\\&+ \frac{b_4}{2}\hat{Q}^2(t) + \frac{b_5}{2\gamma_1}q^2(t) + \frac{b_6}{2\gamma_1}r^2(t),\end{aligned} \tag{56}$$

where b_i, $i = 1, \ldots, 6$, are the positive parameters that will be determined later. The time derivative of (56) along the solutions of (52)-(53), is

$$\begin{aligned}\dot{V}(t) = {} & -2b_1\lambda_1\int_0^1 e^{-z}S_{11}(z,t)\partial_z S_{11}(z,t)dz\\&- 2b_1\int_0^1 e^{-z}S_{11}(z,t)\int_z^1 \partial_t\hat{K}(z,\xi,t)R_{11}(\xi,t)d\xi dz\\&- 2b_1\int_0^1 e^{-z}S_{11}(z,t)\int_0^1 \partial_t\hat{G}(z,\xi,t)R_{22}(\xi,t)d\xi dz\\&- 2b_1\int_0^1 e^{-z}S_{11}(z,t)\partial_t\hat{\varphi}(z,t)\hat{Q}(t)dz\\&+ 2b_1\int_0^1 e^{-z}S_{11}(z,t)\dot{\hat{\zeta}}(t)\hat{\varphi}(z,t)q(t)dz\\&- 2b_1\int_0^1 e^{-z}S_{11}(z,t)\dot{\hat{c}}(t)\hat{\varphi}(z,t)r(t)dz\\&- 2b_1\Big(\gamma_1 - \hat{\zeta}(t)\Big)\int_0^1 e^{-z}S_{11}(z,t)\hat{\varphi}(z,t)\tilde{Q}(t)dz\\&+ 2\lambda_1\int_0^1 e^{z}R_{12}(z,t)\partial_z R_{12}(z,t)dz\\&+ 2\lambda_2 b_2\int_0^1 e^{z}R_{21}(z,t)\partial_z R_{21}(z,t)dz\\&- 2\lambda_2 b_3\int_0^1 e^{-z}R_{22}(z,t)\partial_z R_{22}(z,t)dz\\&- b_4\Big(\hat{\zeta}(t) + c_1\hat{c}(t)\Big)\hat{Q}^2(t)\\&+ b_4\hat{c}(t)\big(S_{11}(1,t) - R_{22}(1,t)\big)\hat{Q}(t)\\&- b_4\dot{\hat{\zeta}}(t)q(t)\hat{Q}(t) + b_4\dot{\hat{c}}(t)r(t)\hat{Q}(t)\\&+ b_4\Big(\gamma_1 - \hat{\zeta}(t)\Big)\tilde{Q}(t)\hat{Q}(t) - b_5q^2(t)\\&+ \frac{b_5}{\gamma_1}q(t)\hat{Q}(t) + \frac{b_5}{\gamma_1}q(t)\tilde{Q}(t) - b_6r^2(t)\\&- \frac{b_6c_1}{\gamma_1}r(t)\hat{Q}(t) + \frac{b_6}{\gamma_1}r(t)\big(S_{11}(1,t) - R_{22}(1,t)\big).\end{aligned} \tag{57}$$

Applying the Cauchy-Schwartz and Young inequalities to the inverse transformation (50) yields

$$\|R_{11}(t)\|^2 \le \alpha_1\|S_{11}(t)\|^2 + \alpha_2\|R_{22}(t)\|^2 + \alpha_3\hat{Q}^2(t), \tag{58}$$

where the positive constants α_1, α_2 and α_3 depend on the bounded kernels $\hat{\varphi}(z,t)$, $\hat{K}(z,\xi,t)$ and $\hat{G}(z,\xi,t)$. Using (A8)-(A17) in Lemma 3 of Appendix A along with (57) and (58), we have

$$\begin{aligned}\dot{V}(t) \le {} & \Big(1 + b_4^2\bar{c}^2 + 2\lambda_2 b_2 e^1 - \lambda_1 b_1 e^{-1}\Big)S_{11}^2(1,t)\\&- \lambda_1 R_{12}^2(0,t) + \Big(\lambda_2 b_3\alpha^2 - \lambda_2 b_2\Big)R_{21}^2(0,t)\\&+ \Big(1 + b_4^2\bar{c}^2 + 3\lambda_1 e^1 - \lambda_2 b_3 e^{-1}\Big)R_{22}^2(1,t)\\&+ \Big(6 - \lambda_1 b_1\Big)\int_0^1 e^{-z}S_{11}^2(z,t)dz\\&- \lambda_1\int_0^1 e^{z}R_{12}^2(z,t)dz - \lambda_2 b_2\int_0^1 e^{z}R_{21}^2(z,t)dz\\&- \lambda_2 b_3\int_0^1 e^{-z}R_{22}^2(z,t)dz + b_1^2\|\partial_t\hat{\varphi}(t)\|^2\hat{Q}^2(t)\\&+ b_1^2\int_0^1\int_0^1 \big(\partial_t\hat{K}(z,\xi,t)\big)^2 d\xi dz\Big(\alpha_1\|S_{11}(t)\|^2\\&+ \alpha_2\|R_{22}(t)\|^2 + \alpha_3\hat{Q}^2(t)\Big)\\&+ b_1^2\int_0^1\int_0^1 \big(\partial_t\hat{G}(z,\xi,t)\big)^2 d\xi dz\|R_{22}(t)\|^2\\&+ b_1^2\|\hat{\varphi}(t)\|^2\dot{\hat{\zeta}}^2(t)q^2(t) + b_1^2\|\hat{\varphi}(t)\|^2\dot{\hat{c}}^2(t)r^2(t)\\&+ \Big(\frac{1}{2} + 3\lambda_1 e^1 c_1^2 + 2\lambda_2 b_2 e^1 c_1^2\\&+ (\gamma_1 + \bar{\zeta})^2\big(\frac{1}{2}b_4^2 + b_1^2\|\hat{\varphi}(t)\|^2\big)\Big)\\&\times\Big(\frac{1}{1 + q^2(t) + r^2(t)} + \frac{q^2(t) + r^2(t)}{1 + q^2(t) + r^2(t)}\Big)\tilde{Q}^2(t)\end{aligned}$$

$$+\Big(3+3\lambda_1 e^1 c_1^2-b_4\big(\hat{\xi}(t)+c_1\hat{c}(t)\big)\Big)\hat{Q}^2(t)$$
$$+\frac{1}{2}b_4^2\dot{\hat{\xi}}^2(t)q^2(t)+\frac{1}{2}b_4^2\dot{\hat{c}}^2(t)r^2(t)$$
$$+\big((\frac{b_5}{\gamma_1})^2-b_5\big)q^2(t)+\big(\frac{1+c_1^2}{2}(\frac{b_6}{\gamma_1})^2-b_6\big)r^2(t). \tag{59}$$

Choosing the positive parameters b_i as

$$b_6<\frac{2\gamma_1^2}{1+c_1^2},$$
$$b_5<\gamma_1^2,$$
$$b_4\geqslant\frac{3+3\lambda_1 e^1 c_1^2}{\underline{\xi}+c_1\underline{c}},$$
$$b_3\geqslant\frac{1+b_4^2\bar{c}^2+3\lambda_1 e^1}{\lambda_2 e^{-1}},$$
$$b_2\geqslant\alpha^2 b_3,$$
$$b_1\geqslant\max\Big\{\frac{1+b_4^2\bar{c}^2+2\lambda_2 b_2 e^1}{\lambda_1 e^{-1}},\frac{6}{\lambda_1}\Big\}, \tag{60}$$

we have

$$\dot{V}(t)\leqslant-\mu V(t)+\ell_1(t)V(t)+\ell_2(t), \tag{61}$$

where

$$\mu=\min\Big\{\frac{\lambda_1 b_1-6}{b_1},\lambda_1,\lambda_2,\frac{2\big(b_4(\underline{\xi}+c_1\underline{c})-3-3\lambda_1 e^1 c_1^2\big)}{b_4},$$
$$2\gamma_1(1-\frac{b_5}{\gamma_1^2}),2\gamma_1(1-\frac{(1+c_1^2)b_6}{2\gamma_1^2})\Big\},$$
$$\ell_1(t)=\rho\Big((\alpha_1+\alpha_2+\alpha_3)b_1^2\int_0^1\int_0^1\big(\partial_t\hat{K}(z,\xi,t)\big)^2d\xi dz$$
$$+b_1^2\int_0^1\int_0^1\big(\partial_t\hat{G}(z,\xi,t)\big)^2d\xi dz+b_1^2\|\partial_t\hat{\varphi}(t)\|^2$$
$$+b_1^2\|\hat{\varphi}(t)\|^2\dot{\hat{\xi}}^2(t)+b_1^2\|\hat{\varphi}(t)\|^2\dot{\hat{c}}^2(t)$$
$$+2\big(\frac{1}{2}+3\lambda_1 c_1^2 e^1+2\lambda_2 b_2 e^1 c_1^2$$
$$+(\gamma_1+\bar{\xi})^2(\frac{1}{2}b_4^2+c_1^2)\big)\frac{\tilde{Q}^2(t)}{1+q^2(t)+r^2(t)}$$
$$+\frac{1}{2}b_4^2\dot{\hat{\xi}}^2(t)+\frac{1}{2}b_4^2\dot{\hat{c}}^2(t)\Big),$$
$$\rho=\frac{1}{\min\big\{b_1e^{-1},b_2,b_3e^{-1},\frac{b_4}{2},\frac{b_5}{2\gamma_1},\frac{b_6}{2\gamma_1}\big\}}, \tag{62}$$

and

$$\ell_2(t)=\Big(\frac{1}{2}+3\lambda_1 e^1+2\lambda_2 b_2 e^1 c_1^2$$
$$+(\gamma_1+\bar{\xi})^2(\frac{1}{2}b_4^2+c_1^2)\Big)\frac{\tilde{Q}^2(t)}{1+q^2(t)+r^2(t)}. \tag{63}$$

Using (61), along with Lemma 4 and Lemma 5 of Appendix A, we conclude that

$$V(t)\in\mathcal{L}_1\cap\mathcal{L}_\infty,\ \lim_{t\to\infty}V(t)=0. \tag{64}$$

TABLE 3. The simulation parameters of the Rijke tube.

Symbol	Value	Symbol	Value
l	1.4 m	$\bar{\rho}$	1.2 kg/m^3
$\bar{P}$	10^5 Pa	A	0.0046 m^2
c	4.55 $\times 10^3$ W.sec.m/kg	α	-0.95
ζ	1.06 $\times 10^3$ 1/sec	γ	1.4

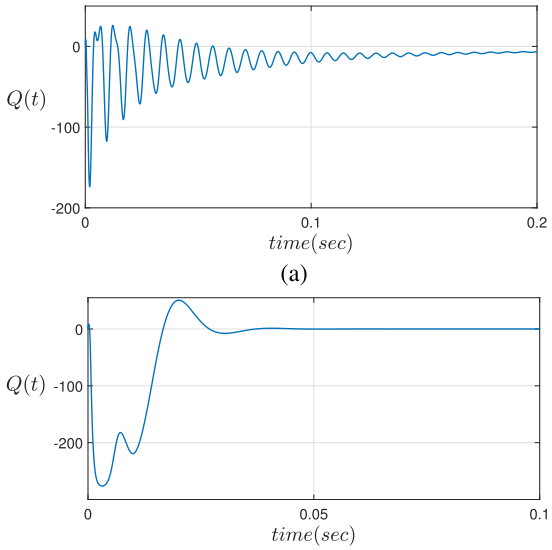

FIGURE 4. Basic performance of the proposed scheme when the coil is located at $x_0=\frac{l}{8}=0.175$: (a) the open-loop response of the heat power release, (b) the closed-loop response of the heat power release. It can be seen that the proposed adaptive scheme accelerates the state convergence to zero.

By $V(t)\in\mathcal{L}_1\cap\mathcal{L}_\infty$, we have

$$\|S_{11}(t)\|^2,\|R_{12}(t)\|^2,\|R_{21}(t)\|^2,\|R_{22}(t)\|^2\in\mathcal{L}_1\cap\mathcal{L}_\infty,$$
$$\hat{Q}^2(t),q^2(t),r^2(t)\in\mathcal{L}_1\cap\mathcal{L}_\infty, \tag{65}$$

which gives the boundedness properties (54). Also, by $\lim_{t\to\infty}V(t)=0$, the regulation properties (55) are obtained.

Step 4: Boundedness and regulation of the system (4)-(5):

In this step, we establish the boundedness and regulation of the closed-loop system given by (42). The boundedness and regulation of $\hat{Q}(t)$, $q(t)$ and $r(t)$ are previously obtained in (54)-(55). Using (24), we get $Q(t)\in\mathcal{L}_2\cap\mathcal{L}_\infty$ and $\lim_{t\to\infty}Q(t)=0$. From (6) and (7), we have

$$\int_0^l R_1^2(x,t)dx=\int_0^{x_0}R_1^2(x,t)dx+\int_{x_0}^l R_1^2(x,t)dx$$
$$=\int_0^1 R_{11}^2(z,t)dz+\int_0^1 R_{21}^2(z,t)dz, \tag{66}$$

therefore,

$$\|R_1(t)\|^2=\|R_{11}(t)\|^2+\|R_{21}(t)\|^2. \tag{67}$$

In a similar manner, we get

$$\|R_2(t)\|^2=\|R_{12}(t)\|^2+\|R_{22}(t)\|^2. \tag{68}$$

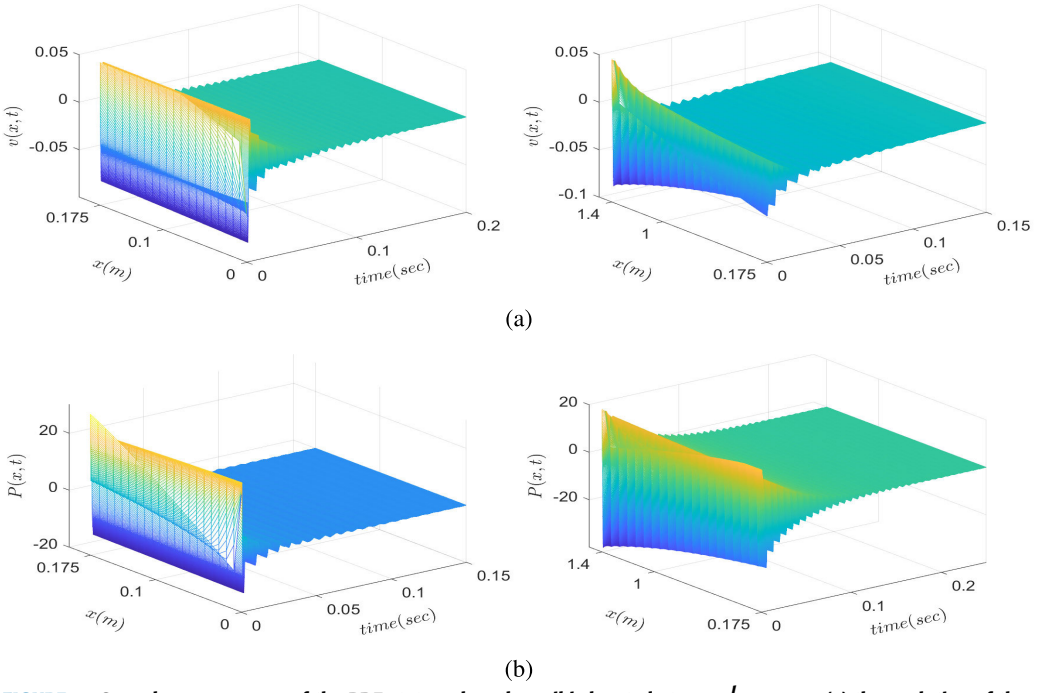

FIGURE 5. Open-loop responses of the PDE states when the coil is located at $x_0 = \frac{l}{8} = 0.175$: (a) the evolution of the acoustic velocity $v(x, t)$, (b) the evolution of the acoustic pressure $P(x, t)$. Note that the spatial domain x in (a) and (b) is broken into two intervals, before and after the discontinuity point $x_0 = 0.175$. It can be seen that the open-loop system has oscillating responses that converge to zero after a relatively long time.

Using (58) and the results of (54)-(55), we get $\|R_{11}(t)\| \in \mathcal{L}_2 \cap \mathcal{L}_\infty$ and $\lim_{t\to\infty} \|R_{11}(t)\| = 0$. Therefore, with the help of (67)-(68) along with (54)-(55), we arrive at $\|R_i(t)\| \in \mathcal{L}_2 \cap \mathcal{L}_\infty$ and $\lim_{t\to\infty} \|R_i(t)\| = 0$, for $i = 1, 2$. This completes the proof of Theorem 1. ■

VI. SIMULATION RESULTS

In this section, we numerically illustrate the basic performance of the proposed scheme along with its ability to handle the additive disturbances, nonlinearities of the model, and the actuator dynamics. To this end, we select the model parameters of the Rijke tube according to Table 3. The initial conditions of the plant are $Q(0) = 2$, $\big(R_1(x, 0), R_2(x, 0)\big) = \big(70\sin(x), -20\sin(x)\big)$ for $x < x_0$, and $\big(R_1(x, 0), R_2(x, 0)\big) = \big(10\sin(x), 50\sin(x)\big)$ for $x > x_0$.

A. BASIC PERFORMANCE

In this section, a simulation example is presented to evaluate the basic performance of the proposed adaptive scheme. The simulation is performed for two cases of the heater coil positions. The adaptive identifier parameters are set to $\gamma_1 = 2$, $\mu_1 = 500$ and $\mu_2 = 100$. The initial conditions of the identifier are $q(0) = 0.1$ and $r(0) = 0.2$, and the initial estimates are $\hat{\zeta}(0) = 1300$ and $\hat{c}(0) = 3700$. The simulation study cases are as follows.

Case 1: The heater coil is located at $x_0 = \frac{l}{8} = 0.175$, which results in $\lambda_1 = 1951.8$ and $\lambda_2 = 278.82$. The open-loop response and the closed-loop response of the ODE state $Q(t)$ are shown in Figs. 4 (a) and (b), respectively. It can be seen that the open-loop system has oscillating behavior that converges to zero after a relatively long time. However, the proposed adaptive scheme accelerates the state convergence to zero. The responses of the PDE states $v(x, t)$ and $P(x, t)$ for the open-loop system and the closed-loop system are shown in Figs. 5 and 6, receptively. Note that the spatial domain x is broken into two intervals, before and after the discontinuity point $x_0 = 0.175$. It can be seen that the proposed adaptive scheme effectively cancels the oscillating behavior of the open-loop system and accelerates the PDE states convergence to zero. Figs. 7 (a) and (b) show the evolution of the control law and the identifier error $\tilde{Q}(t) = Q(t) - \hat{Q}(t)$, receptively. It can be seen that the proposed method is successful and the identifier error converges to zero. The online estimates of the unknown parameters ζ and c, and the parameter estimation errors $\tilde{\zeta}(t)$ and $\tilde{c}(t)$ are shown in Figs. 8 (a) and (b), respectively. As expected, the parameter estimates do not converge to the true values, since the adaptive regulation problem does not ensure the persistence of excitation for parameter convergence. However, the parameter estimation errors are bounded according to (30).

Case 2: The position of the heater coil is $x_0 = \frac{3l}{8} = 0.525$, which results in $\lambda_1 = 650.6$ and $\lambda_2 = 390.36$. The open-loop response and the closed-loop response of the ODE state $Q(t)$ are shown in Figs. 9 (a) and (b), respectively. It can be seen that the open-loop system is unstable and the proposed adaptive scheme effectively stabilizes the system. The results of the simulations for the PDE states $v(x, t)$ and $P(x, t)$ of the open-loop system and the closed-loop system

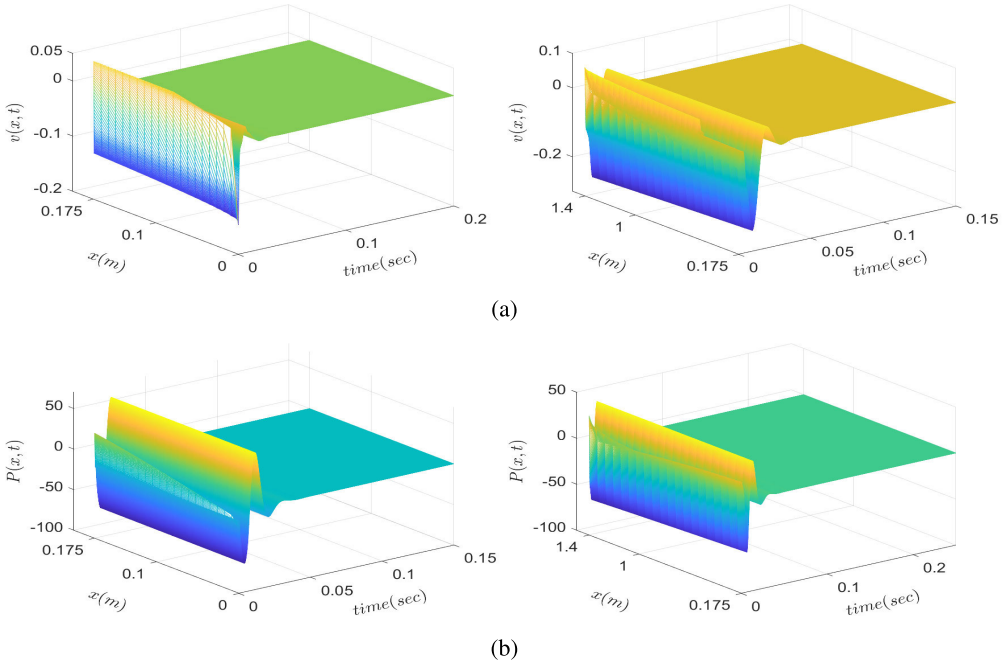

FIGURE 6. Closed-loop responses of the PDE states when the coil is located at $x_0 = \frac{l}{8} = 0.175$: (a) the evolution of the acoustic velocity $v(x,t)$, (b) the evolution of the acoustic pressure $P(x,t)$. Note that the spatial domain x in (a) and (b) is broken into two intervals, before and after the discontinuity point $x_0 = 0.175$. Compared with Fig. 5, it can be seen that the proposed adaptive scheme effectively reduces oscillations along the tube and accelerates the state convergence to zero.

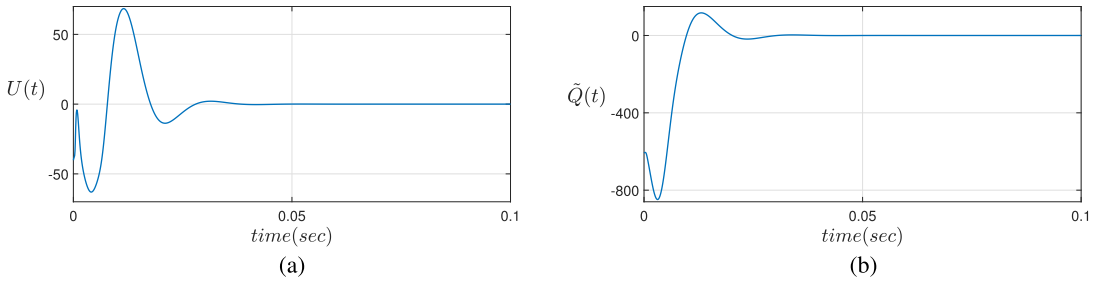

FIGURE 7. Basic performance of the proposed scheme when the coil is located at $x_0 = \frac{l}{8} = 0.175$: (a) the evolution of the control law $U(t)$, (b) the identifier error $\tilde{Q}(t)$. The proposed method is successful and the identifier error converges to zero.

are presented in Figs. 10 and 11, receptively. We can see that the PDE states of the uncontrolled plant quickly grow, however, with the proposed adaptive scheme, the instability is quickly suppressed and the PDE states converge to the zero equilibrium. The control effort $U(t)$ and the identifier error $\tilde{Q}(t)$ are shown in Figs. 12 (a) and (b), respectively. One can see that the identifier error is quickly brought to zero. The estimates of the unknown parameters and the parameter estimation errors are shown in Figs. 13 (a) and (b), respectively. Due to the lack of persistency of excitation in the adaptive regulation problem, the estimation of parameters do not converge to the true values. However, the parameter estimation errors are bounded according to (30).

B. ROBUSTNESS PERFORMANCE

To present the control design and its stability analysis more clearly, this paper only deals with the parametric uncertainties of the Rijke tube model under the assumption that the plant is free of disturbances and nonlinearities. In this section, we numerically illustrate the ability of the proposed scheme to handle the additive disturbances, nonlinearities of the model, and the actuator dynamics.

1) DISTURBANCE ATTENUATION

In this section, we numerically demonstrate the disturbance attenuation property of the proposed adaptive scheme. To this end, we assume that the heat release dynamics of the Rijke tube model is affected by an additive disturbance $d(t)$. In this case, the system is described by

$$\begin{aligned}
&\partial_t R_1(x,t) + \lambda \partial_x R_1(x,t) = \frac{\gamma - 1}{A}\delta(x - x_0)Q(t),\\
&\partial_t R_2(x,t) - \lambda \partial_x R_2(x,t) = \frac{\gamma - 1}{A}\delta(x - x_0)Q(t),\\
&\dot{Q}(t) = -\zeta Q(t) + c\big(R_1(x_0,t) - R_2(x_0,t)\big) + d(t),
\end{aligned} \tag{69}$$

with the boundary conditions

$$R_1(0,t) = -R_2(0,t) + 2U(t),\ R_2(l,t) = \alpha R_1(l,t). \tag{70}$$

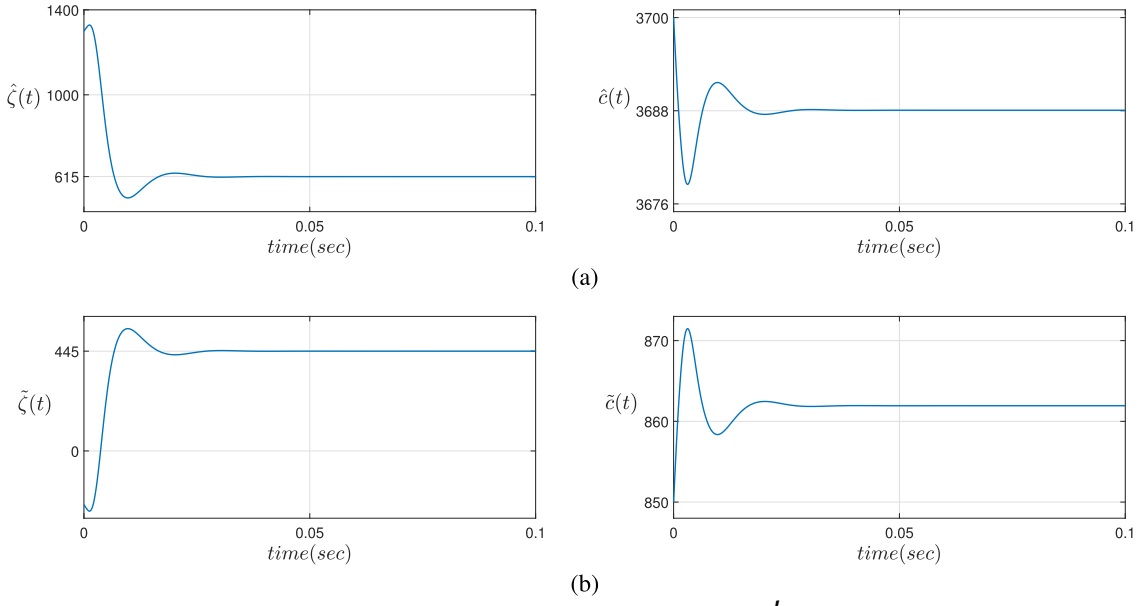

FIGURE 8. Basic performance of the proposed scheme when the coil is located at $x_0 = \frac{l}{8} = 0.175$: (a) the online estimates of the unknown parameters ζ and c whose true values are $\zeta = 1060$ and $c = 4550$, (b) the parameter estimation errors $\tilde{\zeta}(t)$ and $\tilde{c}(t)$. As expected, the parameter estimates do not converge to the true values, since the adaptive regulation problem does not ensure the persistence of excitation for parameter convergence. However, the parameter estimation errors are bounded according to (30).

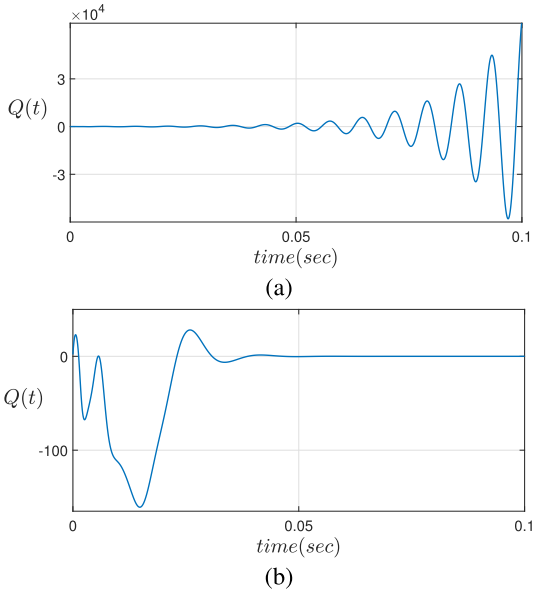

FIGURE 9. Basic performance of the proposed scheme when the coil is located at $x_0 = \frac{3l}{8} = 0.525$: (a) the open-loop response of the heat power release, (b) the closed-loop response of the heat power release. It can be seen that the open-loop system is unstable, and the proposed adaptive scheme effectively stabilizes the system.

The disturbance $d(t)$ is assumed to have a uniform distribution in the range $[-5, 5]$. The adaptive identifier parameters are set to $\gamma_1 = 2$, $\mu_1 = 500$ and $\mu_2 = 100$. The initial conditions of the identifier are $q(0) = 0.1$ and $r(0) = 0.2$, and the initial estimates are $\hat{\zeta}(0) = 1300$ and $\hat{c}(0) = 3700$. The simulation results are presented in Figs. 14–16. The results confirm the desirable disturbance attenuation of the proposed adaptive scheme with a high degree of immunity to the additive disturbance.

2) EFFECT OF NONLINEARITIES AND UNMODELED DYNAMICS

In this section, we study the effectiveness of the proposed scheme when it applies to a more complex model with nonlinear heat release dynamics. To this end, we assume the heat release power is described by the nonlinear ODE [2]

$$\tau \dot{Q}(t) = -Q(t) + l_w(T_w - \bar{T}_{gas})(\kappa + \kappa_v\sqrt{|v(x_0, t)|}). \quad (71)$$

Moreover, we take into account the actuator dynamics which can be regarded as a source of uncertainty in practice. To this end, we assume the control law takes the form of

$$\begin{aligned} U(t) = H(s)\Big\{ &\frac{1}{2}R_2(0,t) - \frac{1}{2}c_1 e^{-\frac{\hat{\zeta}(t)}{\lambda_1}}\hat{Q}(t) \\ &- \frac{1}{2}c_1\hat{c}(t)\int_{t-\frac{1}{\lambda_1}}^{t} e^{-(t-\sigma)\hat{\zeta}(t)}R_1(0,\sigma)d\sigma \\ &+ \frac{1}{2}c_1\hat{c}(t)\int_{t-\frac{1}{\lambda_2}}^{t-\frac{1}{\lambda_2}+\frac{1}{\lambda_1}} e^{-(t-\theta+\frac{1}{\lambda_1}-\frac{1}{\lambda_2})\hat{\zeta}(t)}R_2(l,\theta)d\theta\Big\}, \end{aligned} \quad (72)$$

where s denotes the Laplace variable, and the notation $H(s)\{\cdot\}$ represents the time domain output of a system with the transfer function $H(s)$. In fact, we assume the proposed control law (39) goes through a linear ODE with transfer function $H(s)$ acting as an actuator dynamics. We set the model parameters to $\tau = 0.94 \times 10^{-3}$ sec, $l_w = 1.1$ m, $T_w = 993$ K, $\bar{T}_{gas} = 287.35$ K, $\kappa = 0.026$, $\kappa_v = 0.005$ and $x_0 = \frac{3l}{8} = 0.525$. It is assumed that the actuator dynamics is described by the transfer function $H(s) = \frac{5}{s+5}$. The adaptive identifier parameters are set to $\gamma_1 = 200$, $\mu_1 = 500$ and $\mu_2 = 100$. The initial conditions of the identifier are $q(0) = 1$ and

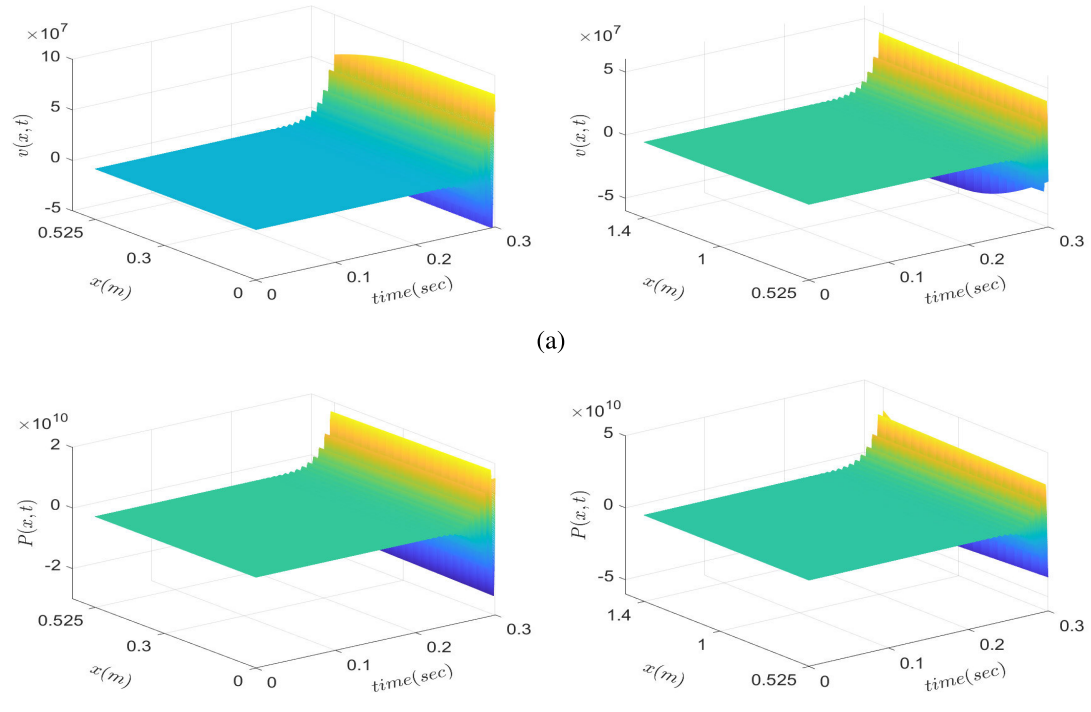

FIGURE 10. Open-loop responses of the PDE states when the coil is located at $x_0 = \frac{3l}{8} = 0.525$: (a) the evolution of the acoustic velocity $v(x,t)$, (b) the evolution of the acoustic pressure $P(x,t)$. Note that the spatial domain x in (a) and (b) is broken into two intervals, before and after the discontinuity point $x_0 = 0.525$. It can be seen that the PDE states of the uncontrolled plant quickly grow.

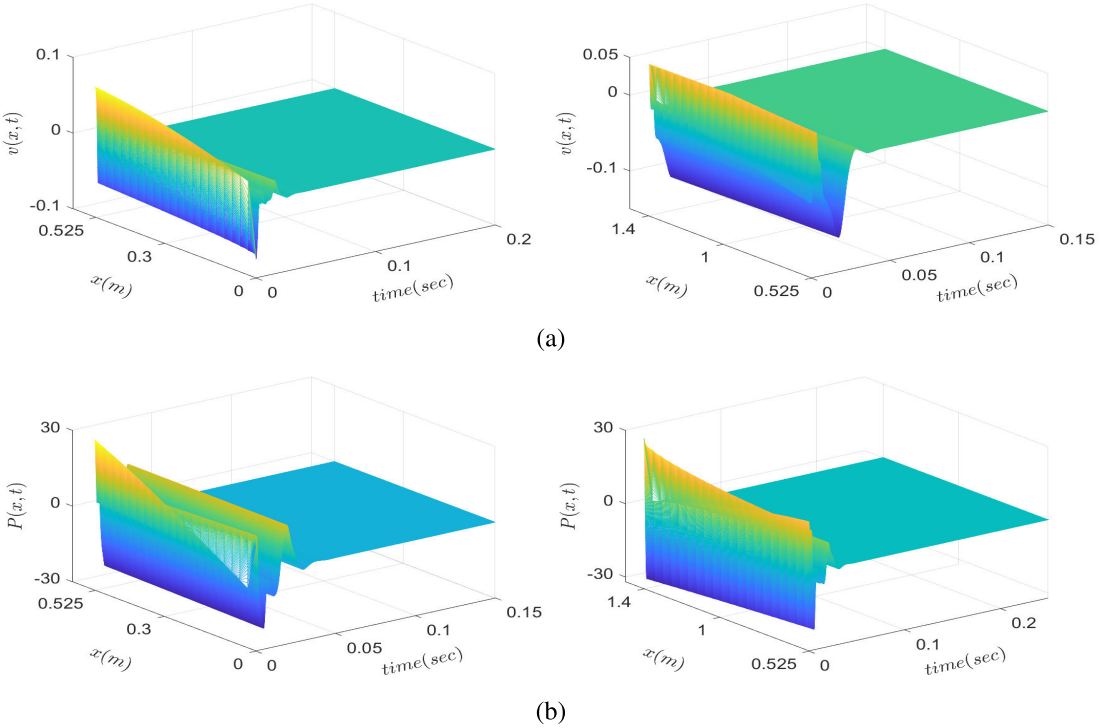

FIGURE 11. Closed-loop responses of the PDE states when the coil is located at $x_0 = \frac{3l}{8} = 0.525$: (a) the evolution of the acoustic velocity $v(x,t)$, (b) the evolution of the acoustic pressure $P(x,t)$. Note that the spatial domain x in (a) and (b) is broken into two intervals, before and after the discontinuity point $x_0 = 0.525$. Compared with Fig. 10, it can be seen that with the proposed adaptive scheme, the instability is quickly suppressed and the PDE states converge to the zero equilibrium.

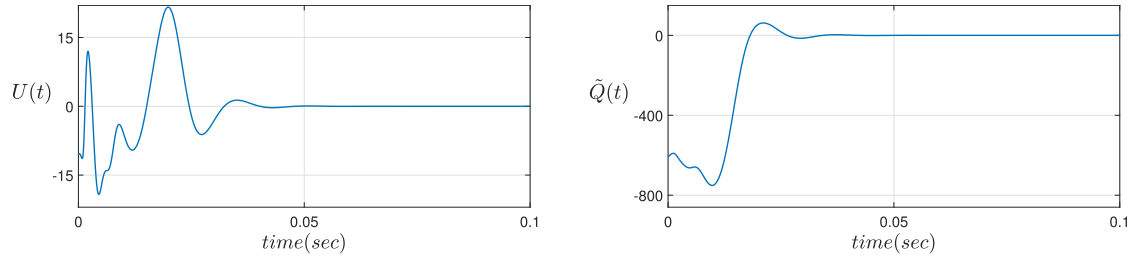

FIGURE 12. Basic performance of the proposed scheme when the coil is located at $x_0 = \frac{3l}{8} = 0.525$: (a) the evolution of the control law $U(t)$, (b) the identifier error $\tilde{Q}(t)$. The proposed method is successful and the identifier error is quickly brought to zero.

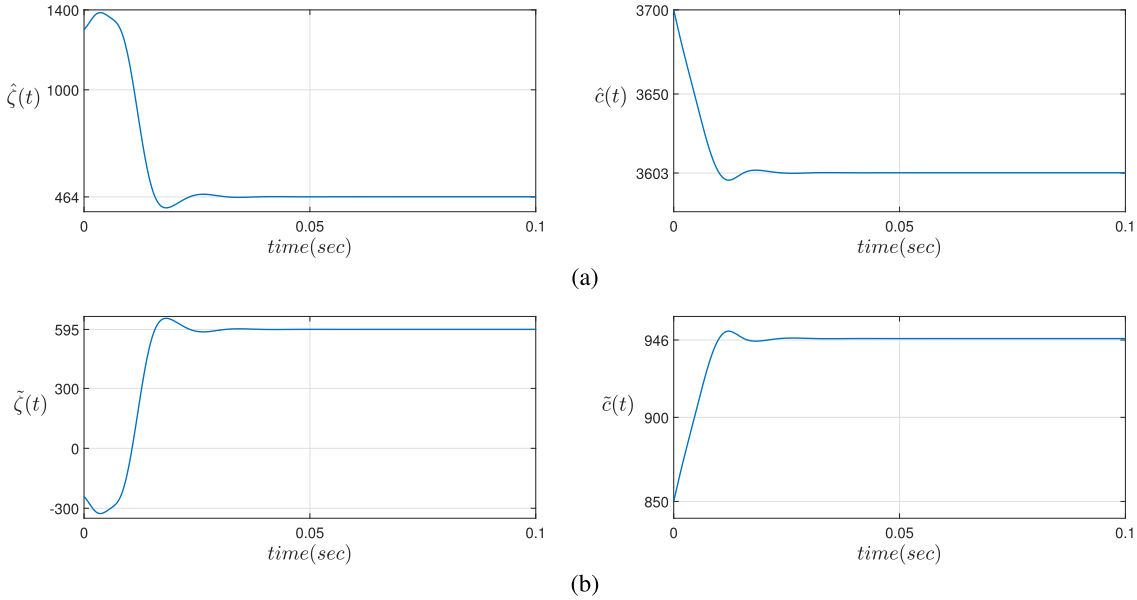

FIGURE 13. Basic performance of the proposed scheme when the coil is located at $x_0 = \frac{3l}{8} = 0.525$: (a) the online estimation of the unknown parameters ζ and c whose true values are $\zeta = 1060$ and $c = 4550$, (b) the parameter estimation errors $\tilde{\zeta}(t)$ and $\tilde{c}(t)$. Due to the lack of the persistency of excitation in the adaptive regulation problem, the estimation of parameters do not converge to the true values. However, the parameter estimation errors are bounded according to (30).

$r(0) = 2$, and the initial estimates are $\hat{\zeta}(0) = 1300$ and $\hat{c}(0) = 3700$. The simulation results are presented in Figs. 17–19. It is worth mentioning that the steady state solution of (71) is $Q^* = l_w(T_w - \bar{T}_{gas})\kappa = 18.46$, and we plot the deviation of $Q(t)$ from Q^* in Fig. 17 (a). It can be seen that the proposed adaptive controller successfully stabilizes the system despite the coexistence of the nonlinear heat release dynamical model and actuator dynamics.

VII. CONCLUSION AND FUTURE WORKS

In this paper, we have presented an adaptive control design for stabilizing the thermoacoustic instability of the Rijke tube described by an ODE-PDE system with the most common uncertain parameters in practice. The stability analysis based on the backstepping method ensures the boundedness and regulation to zero of the ODE-PDE states. The proposed adaptive scheme can be easily implemented since it requires only a few measurements of velocity and pressure along the tube. The numerical simulations illustrate the effectiveness of the proposed scheme when it applies to a more complex model including additive disturbances, nonlinear heat dynamics, and actuator dynamics. To conclude this paper, we briefly highlight some limitations and future opportunities for extending the results of this article.

- In this paper, the adaptive controller is designed based on the linearized ODE-PDE Rijke tube model. In future work, the control design would be extended for a more accurate model including nonlinearities.
- In this paper, the effects of actuator dynamics and external disturbances are studied via simulation examples. However, the stability proof of such cases remains open which can be investigated for future research.
- In this paper, the adaptive stabilization of the ODE-PDE Rijke tube model is achieved by a continous-in-time control law. It would be desirable to design a suitable sampling scheme which ensures the closed-loop stability.

APPENDIX A

Lemma 1: The signal $\epsilon(t)$ in (24) exponentially converges to zero.

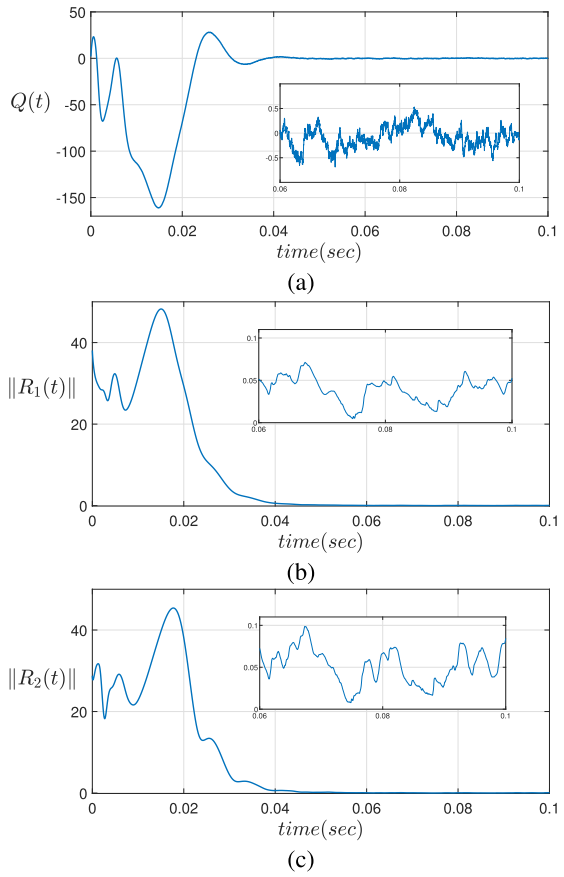

FIGURE 14. Disturbance attenuation property of the proposed scheme when the heat release dynamics is affected by an additive disturbance according to (69); the time responses of: (a) the heat power release $Q(t)$, (b) the spatial L_2-norm of $R_1(x,t)$, (c) the spatial L_2-norm of $R_2(x,t)$. The results confirm the desirable disturbance attenuation of the proposed adaptive scheme with a high degree of immunity to the additive disturbance.

Proof: From (24), we have $\epsilon(t) = Q(t) - (\gamma_1 - \zeta)q(t) + cr(t)$. By taking the time derivative of $\epsilon(t)$ and substituting dynamics of ODE system (18) and filters (23), we obtain

$$\begin{aligned}\dot{\epsilon}(t) &= \dot{Q}(t) - (\gamma_1 - \zeta)\dot{q}(t) - c\dot{r}(t)\\ &= -\gamma_1 Q(t) + \gamma_1(\gamma_1 - \zeta)q(t) + \gamma_1 cr(t)\\ &= -\gamma_1\epsilon(t),\end{aligned} \tag{A1}$$

which is an exponentially stable system, meaning that $\epsilon(t) \in \mathcal{L}_2 \cap \mathcal{L}_\infty$ and $\epsilon(t)$ tends to zero as t tends to ∞.

Lemma 2: The backstepping transformation (48) maps the system (46)-(47) along with the control law (31) into the target system (52)-(53).

Proof: By taking the time derivative of (48), inserting (46) and using integration by parts, we obtain

$$\begin{aligned}\partial_t S_{11}(z,t) = {}& \partial_t R_{11}(z,t) - \int_z^1 \partial_t \hat{K}(z,\xi,t)R_{11}(\xi,t)d\xi\\ &+ \lambda_1\hat{K}(z,1,t)R_{11}(1,t) - \lambda_1\hat{K}(z,z,t)R_{11}(z,t)\\ &- \lambda_1\int_z^1 \partial_\xi\hat{K}(z,\xi,t)R_{11}(\xi,t)d\xi\\ &- \int_0^1 \partial_t\hat{G}(z,\xi,t)R_{22}(\xi,t)d\xi\\ &+ \lambda_2\hat{G}(z,1,t)R_{22}(1,t) - \lambda_2\hat{G}(z,0,t)R_{22}(0,t)\\ &- \lambda_2\int_0^1 \partial_\xi\hat{G}(z,\xi,t)R_{22}(\xi,t)d\xi\\ &- \partial_t\hat{\varphi}(z,t)\hat{Q}(t) - \hat{\varphi}(z,t)\Big(-\dot{\hat{\zeta}}(t)\hat{Q}(t)\\ &+ \hat{c}(t)\big(R_{11}(1,t) - R_{22}(1,t)\big)\\ &- \dot{\hat{\zeta}}(t)q(t) + \dot{\hat{c}}(t)r(t) + \big(\gamma_1 - \hat{\zeta}(t)\big)\tilde{Q}(t)\Big).\end{aligned} \tag{A2}$$

By taking the spatial derivative of (48), we get

$$\begin{aligned}\partial_z S_{11}(z,t) = {}& \partial_z R_{11}(z,t) + \hat{K}(z,z,t)R_{11}(z,t)\\ &- \int_z^1 \partial_z\hat{K}(z,\xi,t)R_{11}(\xi,t)d\xi\\ &- \int_0^1 \partial_z\hat{G}(z,\xi,t)R_{22}(\xi,t)d\xi - \partial_z\hat{\varphi}(z,t)\hat{Q}(t).\end{aligned} \tag{A3}$$

By using

$$\begin{aligned}&\partial_\xi\hat{K}(z,\xi,t) + \partial_z\hat{K}(z,\xi,t) = 0,\\ &\partial_\xi\hat{G}(z,\xi,t) + \frac{\lambda_1}{\lambda_2}\partial_z\hat{G}(z,\xi,t) = 0,\\ &\lambda_1\partial_z\hat{\varphi}(z,t) - \hat{\zeta}(t)\hat{\varphi}(z,t) = 0,\end{aligned} \tag{A4}$$

and

$$\begin{aligned}&\lambda_1\hat{K}(z,1,t) - \hat{c}(t)\hat{\varphi}(z,t) = 0,\\ &\lambda_2\hat{G}(z,1,t) + \hat{c}(t)\hat{\varphi}(z,t) = 0,\\ &\hat{G}(z,0,t) = 0,\end{aligned} \tag{A5}$$

along with

$$\partial_t R_{11}(z,t) + \lambda_1\partial_z R_{11}(z,t) = 0, \tag{A6}$$

we have

$$\begin{aligned}&\partial_t S_{11}(z,t) + \lambda_1\partial_z S_{11}(z,t)\\ &\quad= -\int_z^1 \partial_t\hat{K}(z,\xi,t)R_{11}(\xi,t)d\xi\\ &\qquad- \int_0^1 \partial_t\hat{G}(z,\xi,t)R_{22}(\xi,t)d\xi - \partial_t\hat{\varphi}(z,t)\hat{Q}(t)\\ &\qquad+ \dot{\hat{\zeta}}(t)\hat{\varphi}(z,t)q(t) - \dot{\hat{c}}(t)\hat{\varphi}(z,t)r(t)\\ &\qquad- \big(\gamma_1 - \hat{\zeta}(t)\big)\hat{\varphi}(z,t)\tilde{Q}(t).\end{aligned} \tag{A7}$$

The remainder equations of (52)-(53) are obtained by substituting $S_{11}(1,t) = R_{11}(1,t) + c_1\hat{Q}(t)$ and the control law (31) into (46)-(47). This completes the proof of Lemma 2.

Lemma 3: For the time-derivative of the Lyapunov function given by (57), the following holds:

$$\begin{aligned}&2\int_0^1 e^{-z}S_{11}(z,t)\partial_z S_{11}(z,t)dz\\ &\quad= e^{-1}S_{11}^2(1,t) + \int_0^1 e^{-z}S_{11}^2(z,t)dz,\end{aligned} \tag{A8}$$

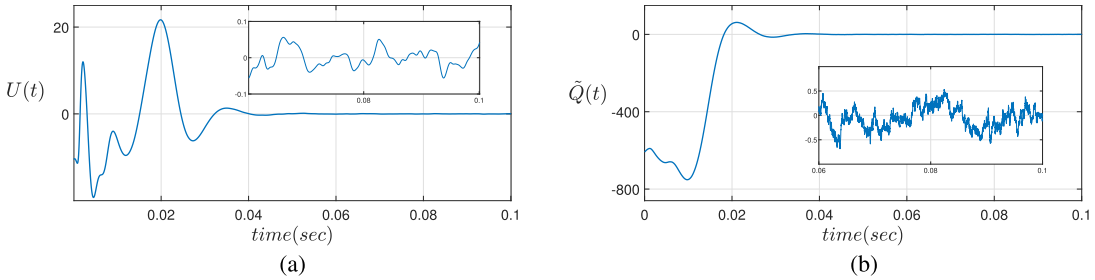

FIGURE 15. Disturbance attenuation property of the proposed scheme when the heat release dynamics is affected by an additive disturbance according to (69): (a) the evolution of the control law $U(t)$, (b) the identifier error $\tilde{Q}(t)$. The proposed method is successful in attenuating the disturbance and the identifier error is brought to zero.

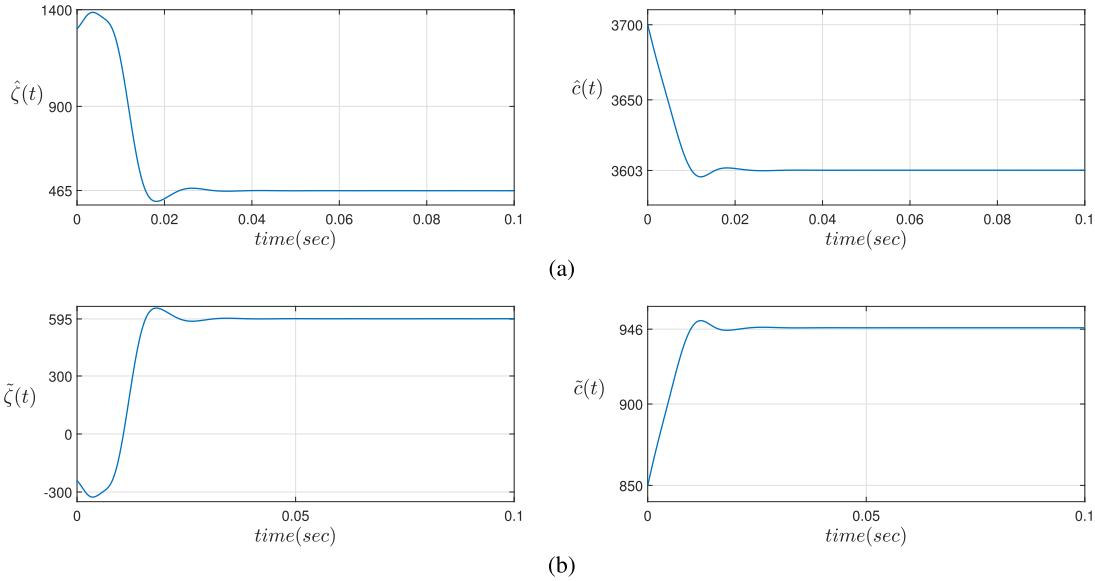

FIGURE 16. Disturbance attenuation property of the proposed scheme when the heat release dynamics is affected by an additive disturbance according to (69): (a) the online estimation of the unknown parameters ζ and c whose true values are $\zeta = 1060$ and $c = 4550$, (b) the parameter estimation errors $\tilde{\zeta}(t)$ and $\tilde{c}(t)$. The errors are bounded according to (30).

$$2\int_0^1 e^{-z}R_{22}(z,t)\partial_z R_{22}(z,t)dz = e^{-1}R_{22}^2(1,t) - \alpha^2 R_{21}^2(0,t) + \int_0^1 e^{-z}R_{22}^2(z,t)dz, \quad \text{(A9)}$$

$$2\int_0^1 e^{z}R_{12}(z,t)\partial_z R_{12}(z,t)dz \leqslant 3\,e^1\left(R_{22}^2(1,t) + c_1^2\hat{Q}^2(t) + c_1^2\tilde{Q}^2(t)\right) - R_{12}^2(0,t) - \int_0^1 e^{z}R_{12}^2(z,t)dz, \quad \text{(A10)}$$

$$2\int_0^1 e^{z}R_{21}(z,t)\partial_z R_{21}(z,t)dz \leqslant 2\,e^1\left(S_{11}^2(1,t) + c_1^2\tilde{Q}^2(t)\right) - R_{21}^2(0,t) - \int_0^1 e^{z}R_{21}^2(z,t)dz, \quad \text{(A11)}$$

$$-2b_1\int_0^1 e^{-z}S_{11}(z,t)\int_z^1 \partial_t\hat{K}(z,\xi,t)R_{11}(\xi,t)d\xi dz \leqslant \int_0^1 e^{-z}S_{11}^2(z,t)dz + b_1^2\left(\int_0^1\int_0^1 \left(\partial_t\hat{K}(z,\xi,t)\right)^2 d\xi dz\right)\|R_{11}(t)\|^2, \quad \text{(A12)}$$

$$-2b_1\int_0^1 e^{-z}S_{11}(z,t)\int_0^1 \partial_t\hat{G}(z,\xi,t)R_{22}(\xi,t)d\xi dz \leqslant \int_0^1 e^{-z}S_{11}^2(z,t)dz + b_1^2\left(\int_0^1\int_0^1 \left(\partial_t\hat{G}(z,\xi,t)\right)^2 d\xi dz\right)\|R_{22}(t)\|^2, \quad \text{(A13)}$$

$$-2b_1\int_0^1 e^{-z}S_{11}(z,t)\partial_t\hat{\varphi}(z,t)\hat{Q}(t)dz \leqslant \int_0^1 e^{-z}S_{11}^2(z,t)dz + b_1^2\|\partial_t\hat{\varphi}(t)\|^2\hat{Q}^2(t), \quad \text{(A14)}$$

$$2b_1\int_0^1 e^{-z}S_{11}(z,t)\hat{\varphi}(z,t)\dot{\hat{\zeta}}(t)q(t)dz \leqslant \int_0^1 e^{-z}S_{11}^2(z,t)dz + b_1^2\|\hat{\varphi}(t)\|^2\dot{\hat{\zeta}}^2(t)q^2(t), \quad \text{(A15)}$$

$$-2b_1\int_0^1 e^{-z}S_{11}(z,t)\hat{\varphi}(z,t)\dot{\hat{c}}(t)r(t)dz \leqslant \int_0^1 e^{-z}S_{11}^2(z,t)dz + b_1^2\|\hat{\varphi}(t)\|^2\dot{\hat{c}}^2(t)r^2(t), \quad \text{(A16)}$$

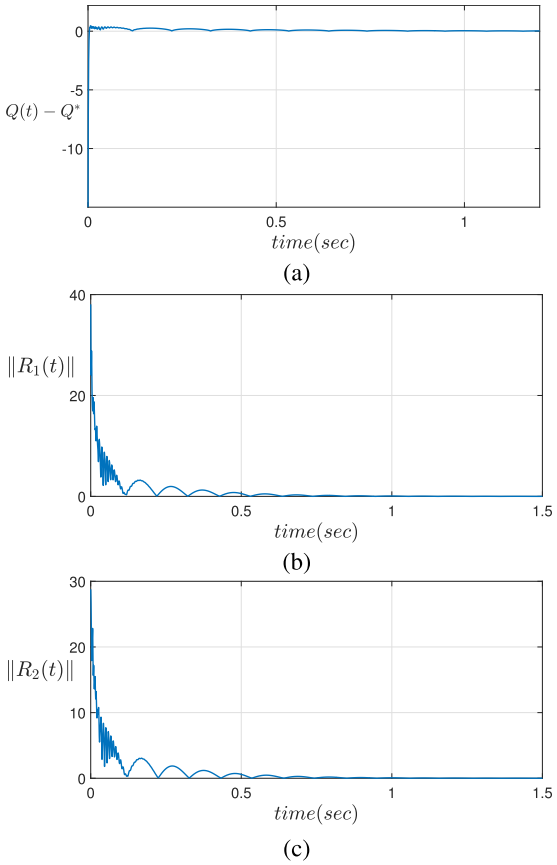

FIGURE 17. Effect of the nonlinearities and actuator dynamics on the performance of the proposed scheme; the time responses of: (a) the heat power release $Q(t)$, (b) the spatial L_2-norm of $R_1(x,t)$, (c) the spatial L_2-norm of $R_2(x,t)$. It can be seen that the proposed adaptive controller successfully stabilizes the system despite the coexistence of the nonlinear heat release dynamical model and actuator dynamics.

$$-2b_1\Big(\gamma_1-\hat{\zeta}(t)\Big)\int_0^1 e^{-z}S_{11}(z,t)\hat{\varphi}(z,t)\tilde{Q}(t)dz$$
$$\leqslant\int_0^1 e^{-z}S_{11}^2(z,t)dz+b_1^2(\gamma_1+\bar{\zeta})^2\|\hat{\varphi}(t)\|^2\tilde{Q}^2(t). \quad \text{(A17)}$$

Proof: (A8) is verified using integration by parts along with $S_{11}(0,t)=0$. Similarly, for (A9), we use integration by parts along with $R_{22}(0,t)=\alpha R_{21}(0,t)$. (A10) is verified using integration by parts along with the inequality

$$R_{12}^2(1,t)\leq 3\Big(R_{22}^2(1,t)+c_1^2\hat{Q}^2(t)+c_1^2\tilde{Q}^2(t)\Big), \quad \text{(A18)}$$

which is obtained by expanding $R_{12}^2(1,t)=\big(R_{22}(1,t)+c_1\hat{Q}(t)+c_1\tilde{Q}(t)\big)^2$ and using the Young inequality. Similarly, (A11) is verified using integration by parts along with the inequality

$$R_{21}^2(1,t)\leq 2\Big(S_{11}^2(1,t)+c_1^2\tilde{Q}^2(t)\Big), \quad \text{(A19)}$$

which is obtained by expanding $R_{21}^2(1,t)=\big(S_{11}(1,t)+c_1\tilde{Q}(t)\big)^2$ and using the Young inequality.
The inequality (A12) is obtained with the help of the Cauchy-Schwartz and Young inequalities as follows

$$-2b_1\int_0^1 e^{-z}S_{11}(z,t)\int_z^1\partial_t\hat{K}(z,\xi,t)R_{11}(\xi,t)d\xi dz$$
$$=-2b_1\int_0^1 e^{-\frac{z}{2}}S_{11}(z,t)\int_z^1 e^{-\frac{z}{2}}\partial_t\hat{K}(z,\xi,t)R_{11}(\xi,t)d\xi dz$$
$$\leq\int_0^1 e^{-z}S_{11}^2(z,t)dz$$
$$+b_1^2\int_0^1 e^{-z}\Big(\int_z^1\partial_t\hat{K}(z,\xi,t)R_{11}(\xi,t)d\xi\Big)^2dz$$
$$\leq\int_0^1 e^{-z}S_{11}^2(z,t)dz$$
$$+b_1^2\int_0^1\int_0^1\big(\partial_t\hat{K}(z,\xi,t)\big)^2d\xi\int_0^1 R_{11}^2(\xi,t)d\xi dz$$
$$\leq\int_0^1 e^{-z}S_{11}^2(z,t)dz$$
$$+b_1^2\int_0^1\int_0^1\big(\partial_t\hat{K}(z,\xi,t)\big)^2d\xi dz\|R_{11}(t)\|^2. \quad \text{(A20)}$$

The inequality (A13) is obtained in a similar manner. The inequality (A14), is obtained with the help of the Cauchy-Schwartz and Young inequalities as follows

$$-2b_1\int_0^1 e^{-z}S_{11}(z,t)\partial_t\hat{\varphi}(z,t)\hat{Q}(t)dz$$
$$=-2b_1\int_0^1 e^{-\frac{z}{2}}S_{11}(z,t)e^{-\frac{z}{2}}\partial_t\hat{\varphi}(z,t)\hat{Q}(t)dz,$$
$$\leq\int_0^1 e^{-z}S_{11}^2(z,t)dz+b_1^2\int_0^1 e^{-z}\big(\partial_t\hat{\varphi}(z,t)\big)^2\hat{Q}^2(t)dz$$
$$\leq\int_0^1 e^{-z}S_{11}^2(z,t)dz+b_1^2\|\partial_t\hat{\varphi}(t)\|^2\hat{Q}^2(t). \quad \text{(A21)}$$

The inequalities (A15)-(A17) are obtained in a similar manner.

Lemma 4: For the functions $\ell_1(t)$ and $\ell_2(t)$ in (62)-(63), we have

$$\ell_1(t),\ell_2(t)\geq 0 \qquad \forall t\geqslant 0,$$
$$\ell_1(t),\ell_2(t)\in\mathcal{L}_1, \quad \text{(A22)}$$

Proof: The positiveness of $\ell_1(t)$ and $\ell_2(t)$ is obvious. From (30), we have $\frac{\tilde{Q}(t)}{\sqrt{1+q^2(t)+r^2(t)}}\in\mathcal{L}_2\cap\mathcal{L}_\infty$. This means that $\frac{\tilde{Q}^2(t)}{1+q^2(t)+r^2(t)}\in\mathcal{L}_1$; subsequently, $\ell_2(t)\in\mathcal{L}_1$. To prove $\ell_1(t)\in\mathcal{L}_1$, we first show the following inequalities

$$\|\partial_t\hat{\varphi}(t)\|^2\leqslant(\frac{c_1}{\lambda_1})^2\dot{\hat{\zeta}}^2(t),$$
$$\|\partial_t\hat{K}(t)\|^2\leqslant 2(\frac{c_1}{\lambda_1})^2\dot{\hat{c}}^2(t)+2(\frac{\bar{c}c_1}{\lambda_1^2})^2\dot{\hat{\zeta}}^2(t),$$
$$\|\partial_t\hat{G}(t)\|^2\leqslant 2(\frac{c_1}{\lambda_2})^2\dot{\hat{c}}^2(t)+2(\frac{\bar{c}c_1}{\lambda_1\lambda_2})^2\dot{\hat{\zeta}}^2(t). \quad \text{(A23)}$$

To this end, by (32), we have

$$\partial_t\hat{\varphi}(z,t)=-c_1\frac{z-1}{\lambda_1}e^{\frac{(z-1)\hat{\zeta}(t)}{\lambda_1}}\dot{\hat{\zeta}}^2(t), \quad \text{(A24)}$$

therefore,

$$\|\partial_t\hat{\varphi}(t)\|^2=\int_0^1\Big(\partial_t\hat{\varphi}(z,t)\Big)^2dz$$

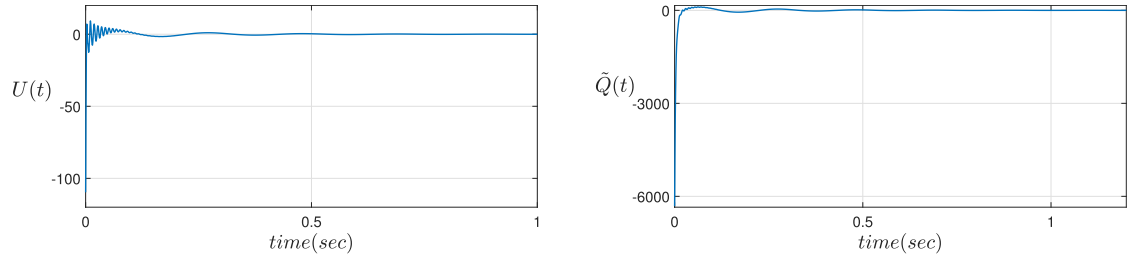

FIGURE 18. Effect of the nonlinearities and actuator dynamics on the performance of the proposed scheme: (a) the evolution of the control law $U(t)$, (b) the identifier error $\tilde{Q}(t)$. The proposed scheme is successful and the identifier error $\tilde{Q}(t)$ converges to zero despite the presence of the nonlinearities and actuator dynamics.

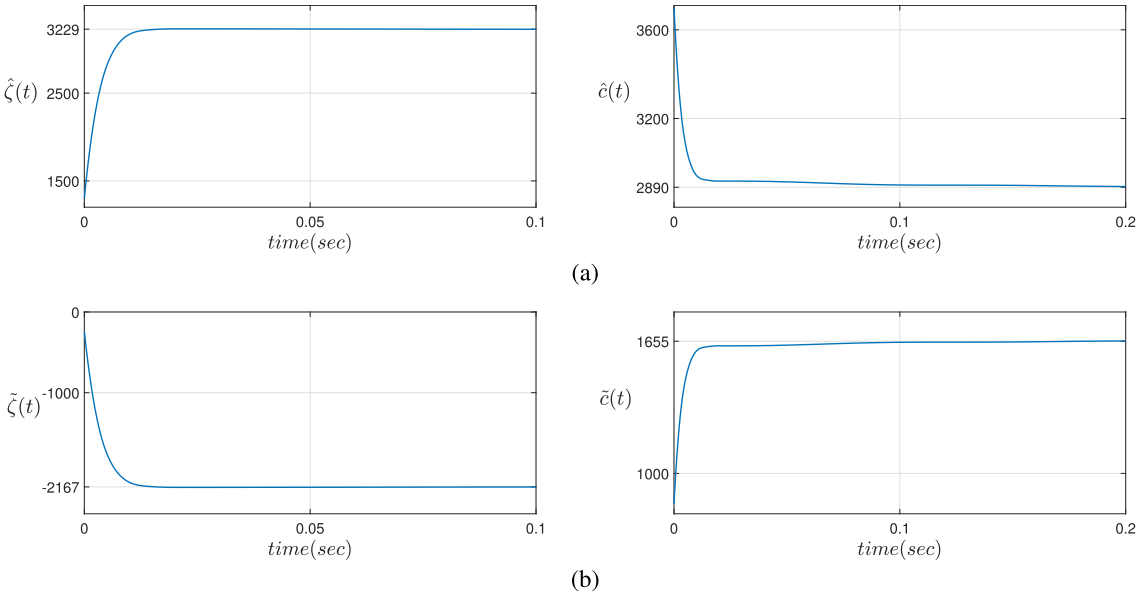

FIGURE 19. Effect of the nonlinearities and actuator dynamics on the performance of the proposed scheme: (a) the online estimation of the unknown parameters ζ and c whose true values are $\zeta = 1060$ and $c = 4550$, (b) the parameter estimation errors $\tilde{\zeta}(t)$ and $\tilde{c}(t)$. The errors are bounded according to (30).

$$\leq \left(\frac{c_1}{\lambda_1}\right)^2 \dot{\hat{\zeta}}^2(t). \tag{A25}$$

In a similar manner, other inequalities of (A23) are obtained. Moreover, from (30), we have $\dot{\hat{\zeta}}(t), \dot{\hat{c}}(t) \in \mathcal{L}_2 \cap \mathcal{L}_\infty$. This means that

$$\dot{\hat{\zeta}}^2(t), \dot{\hat{c}}^2(t) \in \mathcal{L}_1. \tag{A26}$$

Using the expression of $\ell_1(t)$ in (62), along with (A23) and (A26), we conclude that $\ell_1(t) \in \mathcal{L}_1$. This completes the proof of Lemma 4.

Lemma 5 ([40]): Let $V(t)$, $\ell_1(t)$ and $\ell_2(t)$ be real-valued functions defined for $t \geqslant 0$. Suppose

$$\begin{aligned} &V(t), \ell_1(t), \ell_2(t) \geqslant 0 \qquad \forall t \geqslant 0, \\ &\quad \ell_1(t), \ell_2(t) \in \mathcal{L}_1, \\ &\dot{V}(t) \leqslant -\mu V(t) + \ell_1(t)V(t) + \ell_2(t), \end{aligned} \tag{A27}$$

where μ is a positive constant. Then

$$V(t) \in \mathcal{L}_1 \cap \mathcal{L}_\infty, \qquad \lim_{t\to\infty} V(t) = 0. \tag{A28}$$

REFERENCES

[1] A. M. Annaswamy and A. F. Ghoniem, "Active control in combustion systems," *IEEE Control Syst.*, vol. 15, no. 6, pp. 49–63, Dec. 1995.
[2] J. P. Epperlein, B. Bamieh, and K. J. Astrom, "Thermoacoustics and the Rijke tube: Experiments, identification, and modeling," *IEEE Control Syst. Mag.*, vol. 35, no. 2, pp. 57–77, Apr. 2015.
[3] S. M. Sarpotdar, N. Ananthkrishnan, and S. D. Sharma, "The Rijke tube—A thermo-acoustic device," *Resonance*, vol. 8, no. 1, pp. 59–71, Jan. 2003.
[4] F. Pan, X. Cheng, X. Wu, X. Wang, and J. Gong, "Thermodynamic design and performance calculation of the thermochemical reformers," *Energies*, vol. 12, no. 19, p. 3693, Sep. 2019.
[5] G. A. de Andrade, R. Vazquez, and D. J. Pagano, "Backstepping stabilization of a linearized ODE–PDE Rijke tube model," *Automatica*, vol. 96, pp. 98–109, Oct. 2018.
[6] N. Noiray and B. Schuermans, "Theoretical and experimental investigations on damper performance for suppression of thermoacoustic oscillations," *J. Sound Vib.*, vol. 331, no. 12, pp. 2753–2763, Jun. 2012.
[7] G. Gelbert, J. P. Moeck, C. O. Paschereit, and R. King, "Feedback control of unstable thermoacoustic modes in an annular Rijke tube," *Control Eng. Pract.*, vol. 20, no. 8, pp. 770–782, Aug. 2012.
[8] M. A. Heckl, "Active control of the noise from a Rijke tube," *J. Sound Vib.*, vol. 124, no. 1, pp. 117–133, Jul. 1988.
[9] M. Krstic, "Adaptive control of an anti-stable wave PDE," *Dyn. Continuous, Discrete Impuls. Syst.*, vol. 17, no. 6a, pp. 853–882, 2010.
[10] D. Bresch-Pietri and M. Krstic, "Output-feedback adaptive control of a wave PDE with boundary anti-damping," *Automatica*, vol. 50, no. 5, pp. 1407–1415, May 2014.

[11] G. A. Andrade, R. Vazquez, and D. J. Pagano, "Boundary feedback control of unstable thermoacoustic oscillations in the Rijke tube," in *Proc. 2nd IFAC Workshop Control Syst. Governed Partial Differ. Equ.*, Bertinoro, Italy, 2016, pp. 48–53.

[12] A. Smyshlyaev and M. Krstic, *Adaptive Control of Parabolic PDEs*. Princeton, NJ, USA: Princeton Univ. Press, 2010.

[13] P. Bernard and M. Krstic, "Adaptive output-feedback stabilization of non-local hyperbolic PDEs," *Automatica*, vol. 50, no. 10, pp. 2692–2699, Oct. 2014.

[14] H. Anfinsen and O. M. Aamo, "Adaptive output-feedback stabilization of linear 2×2 hyperbolic systems using anti-collocated sensing and control," *Syst. Control Lett.*, vol. 104, pp. 86–94, Jun. 2017.

[15] H. Anfinsen and O. M. Aamo, "Adaptive control of linear 2×2 hyperbolic systems," *Automatica*, vol. 87, pp. 69–82, Jan. 2018.

[16] H. Anfinsen and O. M. Aamo, "Adaptive stabilization of $n + 1$ coupled linear hyperbolic systems with uncertain boundary parameters using boundary sensing," *Syst. Control Lett.*, vol. 99, pp. 72–84, Jan. 2017.

[17] H. Anfinsen and O. M. Aamo, "Adaptive output feedback stabilization of $n + m$ coupled linear hyperbolic PDEs with uncertain boundary conditions," *SIAM J. Control Optim.*, vol. 55, no. 6, pp. 3928–3946, Jan. 2017.

[18] M. Krstic, "Compensating actuator and sensor dynamics governed by diffusion PDEs," *Syst. Control Lett.*, vol. 58, no. 5, pp. 372–377, May 2009.

[19] N. Bekiaris-Liberis and M. Krstic, "Compensation of wave actuator dynamics for nonlinear systems," *IEEE Trans. Autom. Control*, vol. 59, no. 6, pp. 1555–1570, Jun. 2014.

[20] C. Lin and X. Cai, "Boundary control for cascaded system of nonlinear ODE/hyperbolic PDE with time-varying parameter," *IEEE Access*, vol. 9, pp. 104177–104182, 2021.

[21] J. Wang and M. Krstic, "Output-feedback control of an extended class of sandwiched hyperbolic PDE-ODE systems," *IEEE Trans. Autom. Control*, vol. 66, no. 6, pp. 2588–2603, Jun. 2021.

[22] C. Lin and X. Cai, "Stabilization of a class of nonlinear ODE/wave PDE cascaded systems," *IEEE Access*, vol. 10, pp. 35653–35664, 2022.

[23] D. Bresch-Pietri and M. Krstic, "Adaptive trajectory tracking despite unknown input delay and plant parameters," *Automatica*, vol. 45, no. 9, pp. 2074–2081, Sep. 2009.

[24] Y. Zhu, M. Krstic, and H. Su, "Adaptive output feedback control for uncertain linear time-delay systems," *IEEE Trans. Autom. Control*, vol. 62, no. 2, pp. 545–560, Feb. 2017.

[25] J. Li, Y. Liu, and Z. Xu, "Adaptive stabilization for cascaded PDE–ODE systems with a wide class of input disturbances," *IEEE Access*, vol. 7, pp. 29563–29574, 2019.

[26] J. Li and Y. Liu, "Adaptive control of uncertain coupled reaction–diffusion dynamics with equidiffusivity in the actuation path of an ODE system," *IEEE Trans. Autom. Control*, vol. 66, no. 2, pp. 802–809, Feb. 2021.

[27] J. Wang, S.-X. Tang, and M. Krstic, "Adaptive output-feedback control of torsional vibration in off-shore rotary oil drilling systems," *Automatica*, vol. 111, Jan. 2020, Art. no. 108640.

[28] J. Wang, S.-X. Tang, and M. Krstic, "Adaptive control of hyperbolic PDEs coupled with a disturbed and highly uncertain ODE," *IEEE Trans. Autom. Control*, vol. 68, no. 1, pp. 108–123, Jan. 2023.

[29] M. Krstic, *Delay Compensation for Nonlinear, Adaptive, and PDE Systems*. Basel, Switzerland: Birkhauser, 2009.

[30] Y. Zhang, M. Chadli, and Z. Xiang, "Predefined-time adaptive fuzzy control for a class of nonlinear systems with output hysteresis," *IEEE Trans. Fuzzy Syst.*, vol. 31, no. 8, pp. 2522–2531, Aug. 2023.

[31] D. Cui and Z. Xiang, "Nonsingular fixed-time fault-tolerant fuzzy control for switched uncertain nonlinear systems," *IEEE Trans. Fuzzy Syst.*, vol. 31, no. 1, pp. 174–183, Jan. 2023.

[32] W. Wei, J. Wang, D.-H. Li, M. Zhu, H.-J. Tang, and F.-L. Weng, "Dynamic compensation based adaptive control of thermo-acoustic instabilities in Rijke tube: An experimental validation," *ISA Trans.*, vol. 52, no. 3, pp. 450–460, May 2013.

[33] W. MacKunis, M. Reyhanoglu, K. B. Kidambi, and J. R. Hervas, "Robust and adaptive nonlinear regulation of thermoacoustic oscillations in Rijke-type systems," in *Proc. IEEE Int. Conf. Adv. Intell. Mechatronics (AIM)*, Banff, AB, Canada, Jul. 2016, pp. 840–845.

[34] Y. Zhao, D. Ma, and H. Ma, "Adaptive neural network control of thermoacoustic instability in Rijke tube: A fully actuated system approach," *J. Syst. Sci. Complex.*, vol. 35, no. 2, pp. 586–603, Apr. 2022.

[35] J. Paredes and D. Bernstein, "Experimental implementation of retrospective cost adaptive control for suppressing thermoacoustic oscillations in a Rijke tube," *IEEE Trans. Control Syst. Technol.*, vol. 31, no. 6, pp. 2484–2498, Nov. 2023.

[36] S. Chen, R. Vazquez, and M. Krstic, "Bilateral boundary control design for a cascaded diffusion-ODE system coupled at an arbitrary interior point," 2019, *arXiv:1906.04919*.

[37] G. A. de Andrade, R. Vazquez, and D. J. Pagano, "Backstepping-based estimation of thermoacoustic oscillations in a Rijke tube with experimental validation," *IEEE Trans. Autom. Control*, vol. 65, no. 12, pp. 5336–5343, Dec. 2020.

[38] H. Anfinsen and O. M. Aamo, *Adaptive Control of Hyperbolic PDEs*. New York, NY, USA: Springer, 2019.

[39] S. Sastry and M. Bodson, *Adaptive Control: Stability, Convergence, and Robustness*. Upper Saddle River, NJ, USA: Prentice-Hall, 1989.

[40] H. Anfinsen and O. M. Aamo, "A note on establishing convergence in adaptive systems," *Automatica*, vol. 93, pp. 545–549, Jul. 2018.

ELHAM AARABI is currently pursuing the Ph.D. degree in electrical engineering with the Isfahan University of Technology, Isfahan, Iran. Her research interests include adaptive control, control theory, boundary control of partial differential equations, and their applications.

MOHAMMADALI GHADIRI-MODARRES received the Ph.D. degree in electrical engineering from the Isfahan University of Technology, Isfahan, Iran, in 2017.

He is currently an Assistant Professor with the Department of Electrical Engineering, Arak University of Technology, Arak, Iran. His current research interests include adaptive control, extremum-seeking control, time-delay systems, and control of systems described by PDEs.

MOHSEN MOJIRI received the Ph.D. degree in electrical engineering from the Isfahan University of Technology (IUT), Isfahan. Iran, in 2005. From 2006 to 2008, he was a Faculty Member with the Department of Electrical Engineering, Kashan University, Kashan, Iran. Since 2009, he has been with the Department of Electrical and Computer Engineering, IUT, where he is currently an Associate Professor. He also involved in extremum seeking control and its application to multiagent formation. His research interests include adaptive and nonlinear estimation, filtering and control, and signal processing techniques and algorithms as applied to power systems control.